Revisiting the preparation of TiO_2 nanoparticles: A novel protocol with enhanced properties

Thesis submitted in partial fulfilment of the requirements for award of the degree of Master of Engineering in Chemical Engineering

Submitted by

SANKHADEEP BASU

Class Roll No: 001710302011

Examination Roll No: M4CHE19007

Registration No: 123148 of 2013-2014

Under the guidance of

DR. SUDESHNA SAHA

Department of Chemical Engineering

Jadavpur University

Kolkata 700032

2019

Declaration of Originality and Compliance of Academic Ethics

I hereby declare that this thesis contains literature survey and original research work by the undersigned candidate, as part of his "***Master of Chemical Engineering***" studies. All information in this document have been obtained and presented in accordance with academic rules and ethical conduct.
I also declare that, as required by these rules and conduct, I have fully cited and referenced all material and results that are not original to research work.

Name: ***SANKHADEEP BASU***

Examination Roll Number: M4CHE19007

Thesis Title: ***Revisiting preparation of TiO_2 nanoparticles: A novel protocol with enhanced properties***

Signature:

Date:

To whom it may concern

This is to certify that Sankhadeep Basu, final year Master of Chemical Engineering (M.ChE) examination student of Department of Chemical Engineering, Jadavpur University (Exam Roll No: M4CHE19007; Registration No: 123148 of 2013-2014), has completed the project work titled "Revisiting preparation of TiO_2 nanoparticles: A novel protocol with enhanced properties" under the guidance of Dr. Sudeshna Saha in the stipulated time during his post-graduation curriculum. This work has not been reported earlier anywhere and can be approved for submission in partial fulfilment of the course work.

_____ _____

Dr. Sudeshna Saha
Assistant Professor
Chemical Engineering Department
Jadavpur University

Dr. Debashis Roy
Head of Department
Chemical Engineering Department
Jadavpur University

_____

Dr. Chiranjib Bhattacharjee
Dean, Faculty of Engineering & Technology
Jadavpur University

ACKNOWLEDGMENT

It gives great pleasure to express my gratitude to each and everyone who have helped me to complete my research and complete this thesis in the stipulated time. I am grateful to all faculty members of Chemical Engineering Department, Jadavpur University not only for their help in academic matters but also for allowing me to use high end characterization instruments in the department.

I would like to express my very profound gratitude to my guide Dr. Sudeshna Saha for providing me unfailing support and continuous encouragement throughout the two years of study. I could not have imagined having a better advisor for my Master degree research study. This work would not have been possible without her.

I am thankful to my parents who have stood by me in tough times. I am indebted to my lab seniors Sujata Sardar, Samaritri Chattopadhyay, Gourab Ghosh and Rakesh Dey who have continuously motivated me and helped me develop a positive attitude right from my undergraduate days. Without their support this thesis would have been incomplete.

Finally I would like to thank my lab partner Debalina Mondal, seniors Pabitra Baidya and Sibashish Baksi for their help and co-operation.

ABSTRACT

In the present study, two methods of TiO_2 synthesis, namely sol gel and ultrasonication was adopted for preparation of novel C doped nanocrystalline titania. Carbon doping was achieved by modification of the parameters of the conventional synthesis methods and without using external carbon source. For sol gel method, the amount of acid was varied and for sonication method, sonication time period was varied to investigate their effects on the final photocatalyst. Calcination temperature was lower so that the carbon from the precursor can interact with the band gap of TiO_2 and create additional electronic levels. This helped the samples achieve visible light absorption. Photocatalytic activity was evaluated using methylene blue as the model dye. For sol gel method higher acid content led to stable crystalline structure and prevented carbon interaction with TiO_2. For ultrasonic assisted synthesis, higher sonication time failed to lower the band gap. Kinetics followed first order model (L-H model) with highest rate constant value of 0.03169 min^{-1} for sol gel method and 0.0029min^{-1} for sonication method. Low surface area and band gap may be the reason behind such low activity of sonicated TiO_2. All the prepared photocatalyst displayed significant photocatalytic activity in visible range thus showing enhanced performance over conventional white titania.

Contents

1 Introduction 1

1.1 Semiconductor Photocatalysis 1

1.2 Titanium Dioxide 2

1.3 Chemical structure of TiO_2 2

1.4 Applications of TiO_2 5

2 Literature Review 6

2.1 TiO_2 nanopaticles as a photocatalyst 6

2.2 Synthesis of TiO_2 nanoparticles 6

2.2.1 Top down approach 7

2.2.2 Bottom up approach 7

2.3 Mechanism of TiO_2 photocatalysis 13

2.4 Limitations of TiO_2 14

2.5 Strategies for improving TiO_2 photoactivity 15

2.5.1 Morphological modifications 15

2.5.2 Development of visible light active titania photocatalyst 15

2.6 Carbon doped TiO_2 18

2.7 Research Gap 20

2.8 Objectives 21

3 Experimental Methods 22

3.1 Experimental Design 22

3.2 Materials and methods 22

3.3 Preparation of TiO_2 nanoparticles 23

3.4 Characterizations of prepared photocatalyst 24

3.5 Photocatalytic degradation experiments 24

4 Results and Discussion 25

4.1 Characterization of prepared photocatalysts via sol gel and sonication routes 25

4.1.1 XRD analysis 25
4.1.2 FESEM analysis 27
4.1.3 Chemical Analysis 29
4.1.4 FTIR analysis 33
4.1.5 UV-Vis Diffuse Reflectance Spectroscopy 34
4.2 Photocatalytic performance of prepared photocatalysts 37
4.2.1 Effect of synthesis and operating parameters for synthesized TiO_2 37
4.2.2 Kinetics of photocatalytic degradation 40
4.3 Comparison of photocatalyst under ultraviolet, visible and solar radiation 43
4.4 Proposed mechanism of formation of photocatalyst 43
5 Conclusions 46
5.1 Conclusions 46
5.2 Future prospects 47

List of Figures

Figure 1 Rutile, Anatase and Brookite phases 3
Figure 2 Mechanism of TiO_2 photocatalysis 14
Figure 3 Schematic of overall experimental plan 22
Figure 4 XRD patterns of TiO_2 via sol gel route for varying acid amount 26
Figure 5 XRD patterns of TiO_2 via sonication route for varying sonication times 27
Figure 6 FESEM image of sol gel synthesized TiO_2 28
Figure 7 FESEM image of sonication assisted TiO_2 28
Figure 8 Survey spectra for sol gel and sonicated TiO_2 29
Figure 9 Ti 2p deconvolution for sol gel synthesized TiO_2 30
Figure 10 O 1s deconvolution for sol gel synthesized TiO_2 30
Figure 11 C 1s deconvolution for sol gel synthesized TiO_2 31
Figure 12 Ti 2p deconvolution for sonicated TiO_2 31
Figure 13 O 1s deconvolution for sonicated TiO_2 32
Figure 14 C 1s deconvolution for sonicated TiO_2 32
Figure 15 FTIR spectra of TiO_2 nanoparticles synthesized by (a) sol gel and (b) sonication method 33
Figure 16 Model for Kubelka Munk analysis 35
Figure 17 UV-Vis DRS plot for T-0 36
Figure 18 UV-Vis DRS plot for S-0.5 37
Figure 19 Photocatalytic degradation of methylene blue for varying amounts of acid for solgel method 38
Figure 20 Photocatalytic degradation of methylene blue for varying sonication times for sonication method 39
Figure 21 Effect of loading on photocatalytic activity 39
Figure 22 Effect of initial concentration 40
Figure 23 Effect of contact time on photocatalytic degradation 42
Figure 24 Kinetics of photocatalytic degradation 42
Figure 25 Comparison of photocatalyst under ultraviolet, visible and solar radiation 43
Figure 26 UV-Vis DRS spectra for T-0 when calcined at 500°C 45

List of Tables

Table 1 Crystal structure data for TiO_2 4
Table 2 Different methods for synthesis of C doped TiO_2 19
Table 3 Sample Description for sol gel synthesis 23
Table 4 Sample description for ultrasonic synthesis 23
Table 5 Anatase Rutile content calculation 26
Table 6 Band gap from Kubelka Munk function 36

Chapter 1

1 Introduction

1.1 Semiconductor Photocatalysis

Environmental pollution and destruction as well as the lack of sufficient clean and natural energy resources are some of the most serious problems presently faced on a global scale. The increase in world population and the rampant unregulated industrial growth have all led to accelerated energy consumption, while the uncontrolled release of toxic agents and industrial waste into the air and waterways has resulted in pollution-related diseases, global warming, and abnormal climatic changes[1]. Hence it becomes imperative to develop clean energy efficient sustainable technologies for the severe environmental problems, which have become a major concern. Photocatalysis, in which the inexhaustibly abundant, clean, and safe energy of the sun can be harnessed for sustainable, non-hazardous, and economically viable technologies, is a major advance in this direction. Photocatalysis refers to the acceleration of a chemical reaction in the presence of substances called photocatalysts, which can absorb light of appropriate wavelengths depending on the band structure[2], [3]. In photocatalysis, the photocatalyst is activated with either UV light, visible light or a combination of both, and photoexcited electrons are promoted from the valence band to the conduction band, forming an electron/hole pair (e-/h+). The photogenerated pair (e-/h+) is able to reduce and/or oxidize a compound adsorbed on the photocatalyst surface. The general requirements of a photocatalytic system are low band gap, suitable morphology, high surface area, stability and reusability. Semiconductors such as TiO_2, Fe_2O_3, WO_3, ZnO, CeO_2, CdS, ZnS are selected as photocatalysts due to their narrow band gap and distinct electronic structure[4]. However the most important discovery that extensively promoted the field of photocatalysis was the "Honda-Fujishima Effect" first described by Fujishima and Honda in 1972[5]. This well-known chemical phenomenon involves electrolysis of water, which is related to photocatalysis. Photoirradiation of a TiO_2 (rutile) single crystal electrode immersed in an aqueous electrolyte solution induced the evolution of oxygen from the TiO_2 electrode and the evolution of hydrogen from a platinum counter electrode when an anodic bias was applied to the TiO_2 working electrode. Since this pioneering work by Honda/Fujishima, photocatalysis employing various semiconductors, specifically TiO_2, has been the focus of intense investigations by a number of researchers all over the world. Considerable efforts have been

devoted to the design of photocatalytic systems exhibiting a high conversion efficiency of light into chemical energy.

1.2 Titanium Dioxide

Titanium dioxide discovered in 1821, is considered to be one of the top 20 inorganic chemicals of industrial importance[6]. Ever since its commercial production began around 1916, an exponential growth of research has been seen in this area[7]. Titanium dioxide does not occur in nature but is derived from ilmenite or leucoxene ores. It was identified in black sand from Menacchan Valley in Cornwall. German chemist M. H. Klaproth discovered the element in the TiO_2 form, as rutile[8]. The dominant physicochemical properties of TiO_2 nanostructures are classified in terms of their crystallinity, purity, structure, chemical composition, size- and/or shape-distribution, dimensionality and defect centres, which can be easily modified by changing the parameters during various synthetic methods. TiO_2 nanostructures have been widely explored owing to their extensive applications across a myriad of areas, which is discussed in more details in the following sections.

1.3 Chemical structure of TiO_2

TiO_2 belongs to the family of transition metal oxides. There are four commonly known polymorphs of TiO_2 found in nature: anatase (tetragonal), brookite (orthorhombic), rutile (tetragonal), and TiO_2 (B) (monoclinic)[9]. Besides these polymorphs, two additional high-pressure forms have been synthesized from the rutile phase. These are TiO_2 (II) [10] with a PbO_2 structure and TiO_2 (H) [11] with a hollandite structure.

- Rutile: Rutile TiO_2 has a tetragonal structure and contains 6 atoms per unit cell (Figure 1a). The TiO_6 octahedron is slightly distorted[12], [13]. The rutile phase is stable at most temperatures and pressures up to 60 kbar, where TiO_2 (II) becomes the thermodynamically favorable phase. Zhang et al [14] found that anatase and brookite structures transformed to the rutile phase after reaching a certain particle size, with the rutile phase becoming more stable than anatase for particle sizes greater than 14 nm. Once the rutile phase formed, it grew much faster than the anatase. The activity of the rutile phase as a photocatalyst is generally very poor. However, Sclafani et al [15] concluded that the rutile phase can be active or inactive, depending on its preparation conditions.
- Anatase: Anatase TiO_2 also has a tetragonal structure but the distortion of the TiO_6 octahedron is slightly larger for the anatase phase [16], [17], as depicted in Figure 1b.

Muscat et al. [18] found that the anatase phase is more stable than the rutile at 0 K, but the energy difference between these two phases is small (~2 to 10 kJ/mol). The anatase structure is preferred over other polymorphs for solar cell applications because of its higher electron mobility, low dielectric constant and lower density [9]. The increased photoreactivity is because of the slightly higher Fermi level, lower capacity to adsorb oxygen and higher degree of hydroxylation in the anatase phase [19]. Selloni [20] reported that the reactivity of (001) facets is greater than that of (101) facets in an anatase crystal.

- Brookite: Brookite TiO_2 belongs to the orthorhombic crystal system. Its unit cell is composed of 8 formula units of TiO_2 and is formed by edge-sharing TiO_6 octahedral (Figure 1c). It is more complicated, has a larger cell volume and is also the least dense of the 3 forms and is not often used for experimental investigations[16].

The properties of anatase, rutile and brookite forms are listed in Table 1

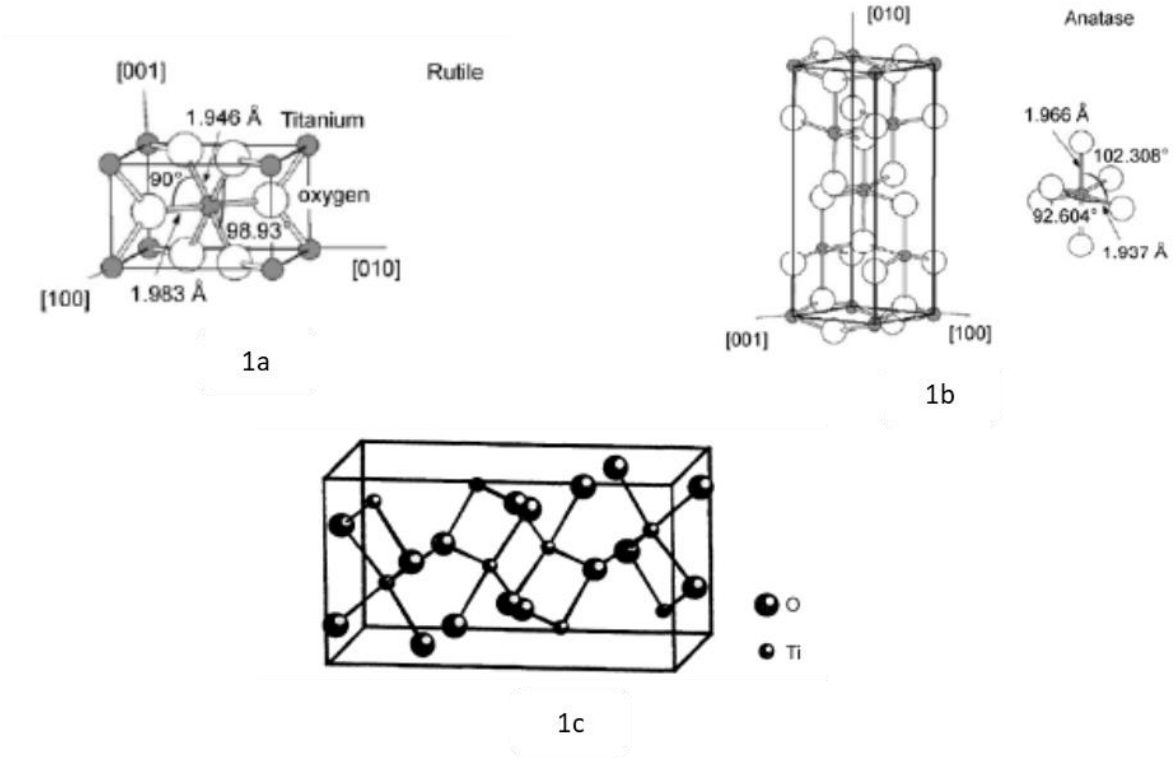

Figure 1 Rutile, Anatase and Brookite phases

Table 1 Crystal structure data for TiO_2

Properties	Rutile	Anatase	Brookite
Crystal structure	Tetragonal	Tetragonal	Orthorhombic
Lattice constant (A)	a = 4.59 c=2.95	a=3.78 c=9.51	a=9.18 b=5.44 c=5.15
Molecule (cell)	2	2	2
Volume/molecule (A)	31.21	34.06	32.17
Density (g/cc)	4.13	3.79	3.99
Ti-O bond length (A)	1.949	1.937	1.87-2.04
O-Ti-O bond angle	81.2° & 90°	77.7° & 92.6°	77°-105°

TiO_2 is a large band semiconductor, with band gaps of 3.2, 3.02, and 2.96 eV for the anatase, rutile and brookite phases, respectively [21]. The valence band of TiO_2 is composed of the 2p orbitals of oxygen hybridized with the 3d orbitals of titanium, while the conduction band is only the 3d orbitals of titanium [22]. When TiO_2 is exposed to near-UV light, electrons in the valence band are excited to the conduction band leaving behind holes (h^+), as shown in Figure 2. The excited electrons (e^-) in the conduction band are now in a purely 3d state and because of dissimilar parity, the transition probability of e^- to the valence band decreases, leading to a reduction in the probability of e^-/h^+ recombination [23]. Anatase TiO_2 is considered to be the active photocatalytic component based on charge carrier dynamics, chemical properties and the activity of photocatalytic degradation of organic compounds. It has inherent surface band bending that forms spontaneously in a deeper region with a steeper potential compared with the rutile phase [24] thus surface hole trapping dominates because spatial charge separation is achieved by the transfer of photogenerated holes towards the surface of the particle *via* the strong upward band bending. However, in the rutile phase, the bulk recombination of electrons and holes occurs, so only holes very close to the surface are trapped and transferred to the surface.

1.4 Applications of TiO_2

The major applications of TiO_2 are as follows

- TiO_2 is an effective opacifier in powder form where it is employed to provide whiteness and opacity to products such as paints, coatings, plastic, paper, inks and even in toothpaste.
- In cosmetic and skin care products, TiO_2 is used both as a pigment, sunscreen and a thickener due to its high refractive index, strong UV light absorption capabilities and its resistance to discoloration under UV light[13][25].
- TiO_2 is widely used for superhydrophobic surfaces, antifogging, self-cleaning surfaces. It also finds use in antibacterial applications
- The most popular use of TiO_2 is as a photocatalyst for various applications such as dye degradation[26]–[28], solar cells[29], production of hydrogen from water[30]–[33], sensors[34], rechargeable batteries[35], super capacitors[36] and environmental remediation[37].
- TiO_2 also finds application in cancer drug delivery[38].

Chapter 2

2 Literature Review

2.1 TiO_2 nanopaticles as a photocatalyst

The primary criteria for an efficient semiconductor photocatalyst are that the redox potential of the charge couple, *i.e.*, e^-/h^+, must lie within the band gap domain of the photocatalyst. The energy level at the bottom of conduction band determines the reducing ability of photoelectrons while the energy level at the top of valence band determines the oxidizing ability of photogenerated holes [39]. The ordinate represents the internal energy not the free energy. The free energy of an e^-/h^+ pair is smaller than the band gap energy because e^-/h^+ pairs have significant configurational entropy arising from the large number of translational states accessible to the mobile carriers in the conduction and valence bands. Apart from possessing suitable band gap energy, an ideal semiconductor should also be easy to produce and use, cost effective, photostable, non-hazardous for humans and the environment, effectively activated by solar light and able to catalyze the reaction effectively. Most of the reported photocatalysts possess limitations, e.g., GaAs, PbS, and CdS are not sufficiently stable for catalysis in aqueous media as they readily undergo photo corrosion and are also toxic[40]. ZnO is unstable because it readily dissolves in water [41] to yield $Zn(OH)_2$ on the ZnO particle surface, which inactivates the catalyst over time. Fe_2O_3, SnO_2, and WO_3 possess a conduction band edge at an energy level below the reversible hydrogen potential, thus systems using these materials require application of an external electrical bias to complete the water splitting reaction and achieve hydrogen evolution at the cathode [42].

TiO_2 is close to being an ideal photocatalyst and the benchmark for photocatalysis performance. TiO_2 is cheap, photo stable in solution and nontoxic. Its holes are strongly oxidizing and redox selective. For these reasons, several novel heterogeneous photocatalytic reactions have been reported at the interface of illuminated TiO_2 photocatalyst, and TiO_2-based photocatalysis has been researched exhaustively for environmental clean-up applications.

2.2 Synthesis of TiO_2 nanoparticles

Synthetic methods of multiphase TiO_2 play a crucial role in the development of nanostructures from zero-dimensional (0D) to three-dimensional (3D) structures. The synthesis of multiphase TiO_2 nanostructures in a variety of shapes with controlled

morphologies, sizes (around 100 nm) and more complex nano-structures are of substantial interest due to their exceptional properties and prevalent application possibilities straddling from physico-chemical to biological fields[43]. With a high degree of synthetic control, the size and shape of multiphase TiO_2 nanostructures can be easily tuned from the micro- and nanometre to the molecular level and from spherical nano-particles to nano-rods/-tubes/-wires. Moreover, owing to its excellent stoichiometry (Ti/O: 1/2), multiphase TiO_2 nano-structures have always been a subject of enormous research interest and there is emerging attention paid now to the controlled synthesis or fabrication of structurally stoichiometric TiO_2 with diverse shapes, with results reported on single and mixed phase TiO_2 polymorphs. The synthesis of multiphase TiO_2 nanostructures, therefore, is very interesting in terms of: (i) the structural phases (anatase-, brookite- and rutile-TiO_2), (ii) the well-controlled morphogenesis (nano-particles, -tubes, -wires, -rods, –crystals and -flowers), and (iii) the particle size (regime 1–100 nm) for a variety of techno-logical and biosafety applications[44].

Generally, two fundamental strategies have been developed to broadly prepare TiO_2 nanostructures: the top-down approach and the bottom-up approach.

2.2.1 Top down approach

Basically, the top-down approach is a miniaturization technique, in which small structures are fabricated from larger ones. The key advantage of this approach are that the components, e.g. in the production of integrated circuits, are both patterned and assembled in position, so that no separate fabrication step is needed. Lithography, attrition or milling, quenching, etching and successive cutting are all typical examples of the top-down approach for the synthesis of metal oxide nanomaterials[45].

2.2.2 Bottom up approach

In this context, synthesis through a bottom-up approach, in which molecular precursors react to form the final larger structures, is a unique approach for the preparation of TiO_2 nanoparticles owing to its exceptional versatility. In the bottom-up approach, the molecular precursors self-associate, interact and combine with each other in a coordinated way to give rise to simple and more complex nanostructures. The bottom-up approach has four major branches: (i) physical, (ii) chemical, (iii) hybrid and (iv) biological. Nowadays, these synthetic routes have been established for the engineering of emerging multi-phase TiO_2 nanostructures (spherical, elongated and planar with sizes smaller than 100 nm)[46]. The existing physical, hybrid and/or biological synthesis methods typically involve toxic

organic/inorganic reagents and need sophisticated instrumentation with complicated reaction conditions to produce the required materials, which are low in quantity as well as quality, even with a low-yield of the required material[47]. Thus, the technological challenge has moved to the facile synthesis of multiphase TiO_2 nanostructures via chemical routes and that could maintain their activity, selectivity and suitability over long-term operation in various potential technological and biosafety applications. In addition, the chemical method is an easy way to produce multiphase-TiO_2 nanostructures using hazardless precursors in a short reaction time and at low cost for high scale-up with high purity in high throughput and good yield in industrial production. Due to numerous advantages such as simplicity, inexpensive instrumental set-up, easy operation and good control over the experimental conditions, the chemical routes are encouraged from the view-point of practical application. The chemical synthesis processes to obtain multiphase crystalline TiO_2 nanostructures, including amongst others sol gel or even hydrothermal approaches, wet chemical solution and precipitation methods, have become increasingly popular in recent years to achieve the goals of identically shaped, uniformly sized, perfect crystals, defect-free and high-purity materials. The bottom up approach provide numerous advantages such as (i) precise control of the structural phases and stoichiometry, (ii) control of the size, morphology and homogeneity, (iii) reproducible process suitable for the large-scale, cost-effective and high-purity production of nanomaterials, (iv) short reaction conditions and inexpensive procedures. Some of the popular synthesis methods are discussed below.

- Sol Gel: The sol– gel method is broadly used to synthesize oxide materials, especially TiO_2 nanomaterials. Processing by this method involves the transformation of a sol (a colloidal suspension of nanometre-sized solid particles in a liquid phase) into a gel (a 3D network of metal– oxygen bonds, containing a continuous solid skeleton attached to a continuous liquid phase), which is then usually thermally treated to obtain the desired material. When the liquid is removed from the sol, the sol turns into a gel. The first gel derived from a metal alkoxide was synthesized by Ebelmen as early as 1846[48]. Amongst all the available processes, the sol– gel approach is mainly based on the controlled hydrolysis, the condensation of appropriate precursors and inorganic polymerization reactions. The sol– gel process includes four steps: (i) hydrolysis, (ii) polycondensation, (iii) drying and (iv) thermal decomposition. The precursors of metal alkoxides hydrolyze with H_2O or alcohols according to the hydrolysis process, followed by either H_2O or alcohol condensation. Additionally, H_2O or alcohol, an

acid or a base can also assist hydrolysis of the precursor. In the case of acids, a reaction takes place between the alkoxide and acid to form a solution. After the sol formation, the solution is condensed to a gel and the solvent (H_2O or alcohol) must be removed. A higher annealing/calcination temperature is needed to decompose the organic/inorganic precursor[5]. Furthermore, the sol– gel method usually results in materials that are amorphous or badly crystalline because they are fabricated at or near room temperature. A thermal treatment (annealing or calcination) is normally needed to transform the gel into the final required crystalline material. The development of Ti-O-Ti chains is favored with low content of water, low hydrolysis rates, and excess titanium alkoxide in the reaction mixture. Three dimensional polymeric skeletons with close packing result from the development of Ti-O-Ti chains. The formation of $Ti(OH)_4$ is favored with high hydrolysis rates for a medium amount of water. The presence of a large quantity of TiOH and insufficient development of three-dimensional polymeric skeletons lead to loosely packed first order particles. Polymeric Ti-O-Ti chains are developed in the presence of a large excess of water [49].From the study on the growth kinetics of TiO_2 nanoparticles in aqueous solution using titanium tetra iso propoxide (TTIP) as precursor, it is found that the rate constant for coarsening increases with temperature due to the temperature dependence of the viscosity of the solution and the equilibrium solubility of TiO_2. Secondary particles are formed by epitaxial self-assembly of primary particles at longer times and higher temperatures, and the number of primary particles per secondary particle increases with time. The average TiO_2 nanoparticle radius increases linearly with time, in agreement with the Lifshitz-Slyozov-Wagner model for coarsening[50].In another study Jiago Yu et al. stated that TiO_2 thin films with different surface structures can be prepared from alkoxide solution containing (PEG) via sol-gel method. Surface structure and photocatalytic activity of the resultant films are mainly dependent on the amount of PEG addition to precursor, larger the amount added to precursor larger the size and no. of pores developed in the resultant films. The transmittance of the film decreases due to the scattering of light by pores of larger size and bigger number in the films. Photocatalytic degradation experiments show that methyl orange is efficiently decolorized in the presence of the TiO_2 thin films by exposing its aqueous solution to ultraviolet light and the suitable surface structures remarkably enhance the photocatalytic activity of TiO_2 films [51]. The photocatalytic activity of TiO_2 films depends on such factors as pore size and number, the amount of

-OH, the surface area and transmittance of TiO_2 films. Transparent TiO_2 thin film photocatalyst was prepared on a SLG substrate via a sol-gel method by Watnabe et al. In this experiment an appreciable amount of sodium diffuses out of a SLG to the TiO_2 layer during the coating process, resulting in a formation of electron-hole recombination center. TiO_2 film formation, leading to a highly photoactive transparent TiO_2 coated SLG, these results are reasonable because photo-induced hydrophilicizing effect is caused by surface structural change of TiO_2 topmost layer. It is considered that although sodium diffusion does decrease total amount of generated electron-hole pairs resulting in decrease in photocatalytic oxidation power, it does not affect topmost surface structural change so much [52].

- Hydrothermal: Hydrothermal synthesis is normally conducted in steel pressure vessels called autoclaves with or without Teflon liners under controlled temperature or pressure with the reaction in aqueous solutions. The temperature can be increased above the boiling point of water and finally reaching the pressure of vapor saturation. The temperature and the amount of solution added to the autoclave are largely responsible for determining the internal pressure produced. It is widely used in the ceramics industry. Hydrothermal synthesis is commonly used to grow synthetic quartz, gems and other single crystals with commercial value. The method has proved to be extremely efficient in the search for new compounds with specific physical properties[53]. For example, TiO_2 nanoparticles were prepared by hydrothermal reaction of titanium alkoxide in an acidic ethanol-water solution, TTIP was added drop wise to mix with ethanol and water solution at pH 0.7 with nitric acid, under this acidic ethanol-water environment were mainly produce primary structure of the anatase phase. The sizes of the particles were controlled to the range of 7-25 nm by adjusting the concentration of Ti precursor and the composition of the solvent system[54]. Besides TiO_2 nanoparticles, TiO_2 nanorods have also been synthesized with the hydrothermal method. Zhang et al. obtained TiO_2 nanorods by treating a dilute TiCl4 solution in presence of acid or inorganic salts. The morphology of the resulting nanorods can be tuned with different surfactants or by changing the solvent compositions [55].
- Sono-chemical method: Ultrasound has been very useful in the synthesis of a wide range of nano structured materials, including high-surface area of transition metals, alloys, carbides, oxides, and colloids. The chemical effects of ultrasound do not come

from a direct interaction with molecular species. A number of different arrangements of equipment have been used for the introduction of the ultrasound irradiation into the electrochemical systems. The first and simplest setup used was made up of a conventional electrochemistry cell, immersed at a fixed position in the ultrasound bath[56]. A lot of studies were carried out using this set up [57] but the power transmitted inside the electrochemistry cell was low and the results depend strongly on its positioning because of heterogeneous distribution of the ultrasound field [58]. Another arrangement is the introduction of an ultrasonic horn system (often referred to as an ultrasonic probe) directly into an electrochemistry cell. This allows the ultrasonic waves to be directed onto the electrode surface and provides much more efficient power control. Various types of sono-electrochemistry cells with ultrasound probes have been reported. Hamed Arami et al. described a procedure to prepare titania nano particles by dissolving TiO_2 pellets into NaOH solution and irradiating the solution in an ultrasonic bath at ambient temperature [59].In another study Jimmy C. Yu et al stated that mesoporous TiO_2 can be synthesized directly under high intensity ultrasound irradiation by using triblock copolymer, brookite phase was formed due to ultra sound irradiation. As a result of using triblock copolymer, the brookite content increased, along with the pore size and crystalline sizes of anatase and brookite [60]. Zhu et al. utilized ultrasonic irradiation process for preparing titania nanotubes, direct sonication of the raw powder and NaOH aqueous solution mixture at high sonicating power, resulted in the formation of titania whisker[58].

- Reverse micelles method: The reverse micelle method has the unique advantage that the numerous nanoscale water pools existing in the micelle suspension are ideal microreactor for synthesizing nanoparticles. The TiO_2 nanoparticles synthesized by using the reverse micelle method were all amorphous hydrates of TiO_2; hence the practical applications of this method were restricted. Micelles and inverse micelles are common method to synthesize TiO_2 nanomaterials. Zhang et al. synthesized Shuttle-like crystalline TiO_2 by hydrolysis of titanium tetrabutoxide in the presence of acids with NP-5 (Igepal CO-520)-cyclohexane reverse micelles at room temperature[61]. The crystal structure, morphology, and particle size of the TiO_2 nanoparticles were largely controlled by the reaction conditions, and the key factors which affected the formation of rutile phase at room temperature included the acidity, the type of acid used, and the microenvironment of the reverse micelles. In another study carried out by Lim et al., TiO_2 nanoparticles were prepared by the controlled hydrolysis of TTIP

in presence of reverse micelles formed in CO_2 with the surfactants of ammonium carboxylate perfluoropolyether and (PDMAEMA-b-PFOMA)[62]. It was found that the crystallite size prepared in the presence of reverse micelles increased as either the molar ratio of water to surfactant or the precursor to surfactant ratio increased.

- Microwave method: Using microwave irradiation it is possible to synthesize nanoparticles with exact parameter control in a short time and also change particle properties and particle size as required. The principal frequencies of microwave heating are between 900 to 2450 MHz. Microwave dielectric heating not only enhances the rate of formation, it also enhances the material quality and size distributions. At lower microwave frequencies, conductive currents flowing within the material due to the movement of ionic constituents can transfer energy from the microwave field to the material. At higher frequencies, the energy absorption is primarily due to molecules with a permanent dipole which tend to re-orientate under the influence of a microwave electric field. Microwave assisted synthesis being faster, cleaner, and more economical than the conventional methods. The fields of application for these produced nanoparticles range from medical uses (drug delivery systems, formulations) to use in many industries, i.e. vehicle manufacturing (coatings, windshields, energy storage), cosmetics (sun protection, shampoo, toothpaste), textile production (outdoor clothing, shoes) and electronics (circuit boards, solar cells, LEDs, touch screens)[63]. Corradi et al. found that colloidal titania particle suspensions can be prepared within 5 min to 1h via microwave radiation, while 1 to 32h was needed for the conventional synthesis method of forced hydrolysis[64]. Nanocrystalline titanium dioxide in the anatase phase has been obtained using urea and $TiOCl_2$ by microwave hydrothermal method. A mixture of urea and $TiOCl_2$ in 5:1 molar ratio is processed in a microwave hydrothermal autoclave for 3 min to precipitate anatase powders; oven-dried powders indicated the formation of single phase anatase in the XRD spectrum[65]. In another study, TiO_2 nanoparticles have been prepared by microwave assisted sol-gel method by annealing the fine powder at 600°C for 1 h[66]. Ma et al. developed high quality rutile TiO_2 nanorods with microwave hydrothermal method & found that they aggregated radially into spherical secondary nanoparticles[67]. Wu et al. synthesized TiO_2 nana tubes by microwave radiation via reaction of anatese, rutile & mixed phase of TiO_2 crystals with NaOH solution under a certain microwave power[68].

2.3 Mechanism of TiO_2 photocatalysis

There are 2 types of photochemical reaction proceeding on a TiO_2 surface when irradiated with UV light, one includes the photo-induced redox reaction of adsorbed substances and the other is photo- induced hydrophilic conversion of TiO_2 itself[69]. With the absorption of photons with energy larger than the band gap of TiO_2, electrons are excited from the valence band to the conduction band, creating electron-hole pairs. These charge carriers migrate to the surface and react with the chemicals adsorbed on the surface to decompose these chemicals[70]. The photo generated holes in the valence band diffuse to the TiO_2 surface & react with adsorbed water molecules, forming hydroxyl radicals (-OH) [71]. The photogenerated holes & the hydroxyl radicals oxidize nearby organic molecules on the TiO_2, followed by electrons in the conduction band which participate in reduction processes, these react with molecular oxygen in the air to produce superoxide radical anion (O_2^-).This photodecomposition process usually involves one or more radicals or intermediate species such as OH, O_2^-, H_2O_2, or O_2, which play important roles in the photocatalytic reaction mechanisms. The photocatalytic activity is largely controlled by (i) the light absorption properties, e.g., light absorption spectrum and coefficient, (ii) reduction and oxidation rates on the surface by the electron and hole, (iii) and the electron-hole recombination rate. A large surface area with a constant surface density of adsorbents leads to faster surface photocatalytic reaction rates, implying larger the specific surface area, the higher the photocatalytic activity is. Higher the crystallinity, fewer is the bulk defects, and higher the photocatalytic activity. High temperature treatment usually improves the crystallinity of TiO_2 nanomaterials, which in turn can induce the aggregation of small nanoparticles and decrease the surface area[72]. Figure shows the general mechanism of TiO_2 photocatalysis.

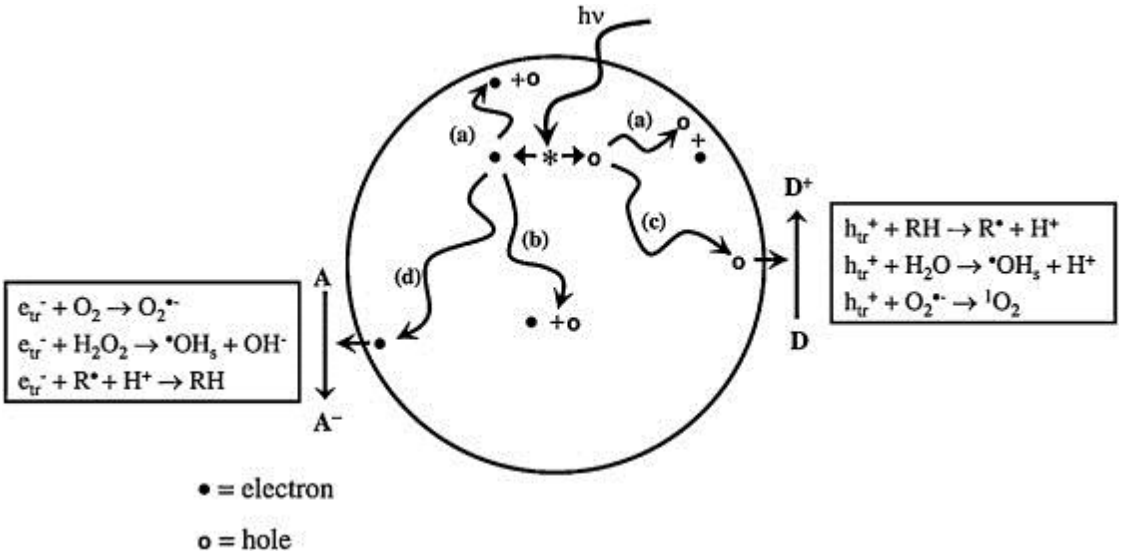

Figure 2 Mechanism of TiO_2 photocatalysis

2.4 Limitations of TiO_2

Despite being one of the efficient photocatalyst, TiO_2 finds limited commercial application due to some inherent drawbacks, which are listed below.

- Anatase has a relatively high band gap of about 3.2eV which is one of the main drawbacks of TiO_2. For photocatalysis light of energy greater than the band gap of the semiconductor, excites an electron from the valence band to conduction band. For anatase UV light of wavelength less than 387nm is required. Hence Anatase has the ability to perform only under ultraviolet radiation of sunlight, which is only 5% of the total spectrum.
- Due to its poor affinity to organic pollutants, the adsorption of organic wastes onto TiO_2 surface is relatively low resulting in slow photocatalytic degradation rates. Since photocatalytic degradation occurs on the surface of TiO_2, mass transfer limitation has to be minimized.
- In most photocatalytic processes, the nanoparticles tend to undergo agglomeration due to the instability of the nanosized particle, which may hamper the light incidence on the active centers and consequently decrease the activity. However it should also be noted that small particles also exhibit higher scattering, which can again reduce the activity compared to large ones.
- One practical challenge to overcome is to recover the nanosized TiO_2 particles from the treated water in regards to both the economic concern and safety concern.

To overcome the limitations, various countermeasures have been proposed by researchers. The purpose of such countermeasures was to improve photocatalytic efficiency, induce visible light absorption, and achieve long term stability to enhance recycle and reuse abilities of TiO_2.

2.5 Strategies for improving TiO_2 photoactivity

2.5.1 Morphological modifications

Various strategies have been adopted for improving the photocatalytic efficiency of TiO_2. They can be summarized as either morphological modification, such as increasing surface area and porosity, or as chemical modification, by incorporation of additional components in the TiO_2 structure. Although visible light active (VLA) TiO_2 photocatalysts require chemical modifications, which will be reviewed in the next section, their overall efficiencies have been significantly enhanced by controlling the semiconductor morphology. The most commonly used TiO_2 morphology is that of monodispersed nanoparticles wherein the diameter is controlled to give benefits from the small crystallite size (high surface area, reduced bulk recombination) without the detrimental effects associated with very small particles (surface recombination, low crystallinity) [73]. One dimensional (1D) titania nanostructures (nanotubes, nanorods, nanowires, nanobelts, nanoneedles) have been also formed by hydrothermal synthesis but high emphasis was given in titania self-assembled nanotubular films grown by electrochemical anodization on titanium metal foils. Advantages of such structures is their tailored morphology, controlled porosity, vectorial charge transfer[74] and low recombination at grain boundaries that result in enhanced performance in photoinduced applications, mainly in photocatalysis[74][75]. An interesting use of TiO_2 nanotubes in photocatalytic applications is the growth of freestanding flow-through membranes[74].

2.5.2 Development of visible light active titania photocatalyst

- Doping with metals: Over the past decades, metal-doped TiO_2 (e.g., Cu, Co, Ni, Cr, Mn, Fe, Ru, Au, Ag, Pt) photocatalysts have been widely studied for improved photocatalytic performance on the degradation of various organic pollutants under visible light irradiation [76], [77][78]. TiO_2 particles can be simply substitutionally or interstitially doped with different cations, can form mixed oxides or a mixture of oxides. The dominant parameters include the character and concentration of dopants and the applied thermal treatment[79]. Many controversial results are reported in the

literature since even the method of doping (e.g., impregnation, coprecipitation, and solegel methods) leads to different morphological and crystalline properties of the photocatalyst[80]. The effect of metal ion dopants on the photocatalytic activity is a complex problem. The visible light photoactivity of metal-doped TiO_2 can be explained by a new energy level produced in the band gap of TiO_2 by the dispersion of metal nanoparticles in the TiO_2 matrix. Electrons can be excited from the defect state to the TiO_2 conduction band by photons with energy equal to hv. An additional benefit of transition metal doping is the improved trapping of electrons to inhibit electron hole recombination during irradiation. Deposition of metal nanoparticles with a large work function, such as Ag[81] onto TiO_2 surface has been found to efficiently retard the e^-h^+ recombination because of the Schottky barrier formed at the metal TiO_2 interface. Decrease of charge carriers recombination results in enhanced photoactivity. Here, the metal nanoparticles act as a mediator in storing and shuttling photogenerated electrons from the TiO_2 surface to an acceptor. Iliev et al. [82]demonstrated that deposition of Pt or Ag on the surface of TiO_2 greatly enhanced the photocatalytic degradation of oxalic acid due to the increased separation of e^-h^+ and higher rate of O_2 reduction. Besides the above causes for the enhanced photoactivity of metal-doped TiO_2, there is another factor that should be taken into account in the photocatalytic process. Since surface sites can also be occupied by metal ion dopants, the surface properties as well as the point of zero charge value of TiO_2 may be altered by doping, depending both on the type and amount of the dopant metal. Consequently, a modification of adsorption properties takes place. However, it was found that the photocatalytic activity of metal-doped TiO_2 could be influenced by dopant concentration. Ambrus et al. [83]reported an improved photocatalytic performance for the optimum Fe dopant concentration. Beyond the optimum concentration of dopant, the photodegradation rate decreased. It was concluded that the dopant ions below an optimum dosage level can act as electron hole separation centres, and thus enhance the photocatalytic efficiency, while the dopant ions with dosage level exceeds optimum value, can act as electron hole recombination centres which are detrimental to the photocatalytic activity. Besides, metal doping showed other drawbacks: thermal instability of doped TiO_2 and requirement of more expensive ion-implantation facilities. In addition, although noble metals coupling could be efficient in improving the photocatalytic reactions, the cost-effectiveness

needed by industrial application usually causes their replacement by more economical transition or non-metals doping.

- Doping with non-metals: Compared with metal dopants, non-metal dopants, such as C, N, S, B, P, F and I [84]may be more appropriate for the extension of the photocatalytic activity of TiO_2 into the visible region because their impurity states are near the valence band edge, but they do not act as charge carriers, and their role as recombination centres might be minimized. Numerous contributions have been devoted recently to developing effective TiO_2 photocatalysts doped with non-metal elements to extend the light absorbance of TiO_2 into the visible region[84], [85]. Among all non-metal-doped TiO_2 materials, N- and C-doped TiO_2 nanomaterials have been found to exhibit superior photocatalytic activity under visible light irradiation. Until now, much effort has been focused on the research of N-doped TiO_2 (N-TiO_2). There have been a large number of publications that deal with the preparation of N-TiO_2 by physical or chemical methods, including sol-gel, sputtering, ion implantation, mechano-chemical and plasma-enhanced chemical vapor deposition method [80]. However, different conclusions concerning the state of doped nitrogen in the N-TiO_2 lattice and the mechanism of band gap narrowing have been derived. For example, Asahi et al.,[86] proposed that substitution-type doping using N was effective for the band gap narrowing of TiO_2 due to the mixing of N 2p with O 2p states in the valence band based on spin restricted local density approximation calculations on anatase. The N 2p state hybrids with O 2p states in anatase TiO_2 doped with nitrogen because their energies are very close, and thus the band gap of N-TiO_2 is narrowed and the material becomes able to absorb visible light. However, Irie et al.,[87] found that interstitial type doping of N atoms was related to the photo-threshold energy decrease, which induced localized N 2p states within the band gap just above the top of the valence band, facilitating the production of oxygen vacancies. Ihara et al. [88] reported that oxygen-deficient sites formed in the grain boundaries is important to emerge vis-activity and nitrogen doped in part of oxygen-deficient sites are important as a blocker for re oxidation. Zhao and Liu [89] concluded that TiO_2 doped with substitutional nitrogen has shallow acceptor states above the valence state. In contrast, TiO_2 doped with interstitial nitrogen has isolated impurity states in the middle of the band gap. These impurity energy levels are mainly hybridized by N 2p states and O 2p states. Besides N-TiO_2, the carbon doped TiO_2 (C-TiO_2) has also received special attention [90]. Sakthivel and Kisch [91]reported that C-TiO_2 was five times more active than

N-TiO_2 in the degradation of 4-chlorophenol by visible light. In the investigation of C-TiO_2, similar to the N-TiO_2, there was also a debate as to whether the doped type of carbon is substitutional or interstitial. This was accounted for by the crystal form and synthesis method of TiO_2.

- Metal deposition: Modifications of TiO_2 with transition metals such as Cr, Co, V and Fe have extended the spectral response of TiO_2 well into the visible region also improving photocatalytic activity. Deposition of noble metals like Ag, Au, Pt and Pd on the surface of TiO_2 enhances the photocatalytic efficiency under visible light by acting as an electron trap, promoting interfacial charge transfer and therefore delaying recombination of the electron‑hole pair[92]. Hwang et al. showed that platinum deposits on TiO_2 trap photo-generated electrons, and subsequently increase the photo-induced electron transfer rate at the interface. Seery et al. showed enhanced visible light photocatalysis with Ag modified TiO_2 [93]. While Gunawan et al. demonstrated the reversible photoswitching of nano silver on TiO_2 where reduced silver on a TiO_2 support exposed to visible light (>450 nm) resulted in excitation and reverse electron flow from silver to the TiO_2 support, oxidising silver ($Ag^0 \rightarrow Ag^+$) in the process[94].
- Coupled semiconductors: Many efforts have been made in the synthesis of different coupled semiconductors such as ZnO/TiO_2, CdS/TiO_2, and Bi_2S_3/TiO_2[92]. The synthesized couples significantly enhance the photocatalytic efficiency by decreasing the recombination rate of the photogenerated electron‑hole pairs and present potential applications in water splitting, organic decomposition, and photovoltaic devices[95]. These composites were also considered as promising materials to develop a high efficiency photocatalyst activated with visible light. They can also compensate the disadvantages of the individual components, and induce a synergistic effect such as an efficient charge separation and improvement of photostability[92]. Therefore, visible light-driven coupled photocatalysts that can decompose organic material are of great interest[96].

2.6 Carbon doped TiO_2

Addition of small amount of carbon impurity to TiO_2 in a controlled manner is referred to as C-doping of titania. The added C-impurity gives the semiconductor TiO_2 an excess of conducting electrons or an excess of conducting holes which is crucial for making visible light active. The white color of the pure titania changed to grey/ black depending on the amount of carbon in titania. The general chemical formula may be represented as TiO_2-x Cx

and the x value varies depending on the preparation condition. The incorporation of carbonaceous species may be responsible for the absorption tail in the visible-light region. The carbons in the doped samples may play the roles, such as(i) it is the sensitizer for visible-light absorption, (ii) it can also be the lattice defect of TiO_2 to form interface states that effectively lower the band gap[97]. Various titanium and carbon precursors that have been used for the preparation of CDT are summarized in Table 2. It is clear from this table, the preparation methods used are hydrolysis followed by thermal treatment, Ti metal burning in flame, oxidative annealing of TiC, spray pyrolysis of Ti and C –precursors and Ti metal sputtering and then RF treatment with CO_2 also utilized. The Ti precursors employed are titanium alkoxides such as tetrabutyl titanate (TBT) and titanium tetra-isopropoxide (TTP), Ti metal, TiCl4, and TiC with carbon sources such as CO, CO2, m ethane, natural gas, hexane, acetylene, alkoxides, carbide and tetrabutyl ammonium hydroxide (TBAH). Heat treatments up to 600°C yield anatase and above 800°C result in the rutile type. Presence of carbon is reported to prevent phase transformation. However, crystal phase depends on the temperature and preparation conditions.

Table 2 Different methods for synthesis of C doped TiO_2

Sl No.	Method of doping	Carbon precursor	Reference
1	Controlled combustion of Ti metal in natural gas flame at 850C	Natural gas	[98]
2	Hydrolysis reaction of TiCl4 and tetrabutyl ammonium hydroxide followed by calcination at 550°C	tetrabutyl ammonium hydroxide	[99]
3	High temperature oxidation of TiC at 350-800°C in air	TiC	[100]
4	TiC oxidative annealing at 800°C for 2 h	TiC	[101]
5	Anodization of titanium foil followed by propane flame annealing for 3 min	Propane	[102]
6	Film deposition on glass plates by sputtering Ti metal under CO_2/Ar gas mixture in a RF magnetron sputtering apparatus	CO_2	[103]
7	TiCl4 & glucose solution spray pyrolysis followed by calcinations in air at 400-850°C for 5-10 min	Glucose	[104]
8	Ti sheet oxidation (flame pyrolysis) with methane	Methane	[105]
9	Hydrolysis of titanium iso-propoxide & heating with glucose at 160°C for 12 h	Glucose	[106]

2.7 Research Gap

Despite the increased use and development in the past decades, TiO_2 based photocatalyst technology still suffers from some major barriers which impede its commercialization. The key research gaps that require more attention are as follows

i. Lack of simple, efficient, cost effective technique for enhancement of visible light photoactivity of TiO_2 limits commercialization. The existing strategies, like doping, for improving visible light activity are expensive, often release undesirable gaseous by-products, and require thermal treatment at high temperatures as well as toxic unstable precursors.

ii. The synthesis procedures for visible light active photocatalysts are energy demanding and tedious which attributes to higher preparation cost resulting large scale application difficult.

iii. Much research has been carried out on photodegradation of organic pollutants by TiO_2 nanoparticles where the end products are carbon dioxide and water. Photocatalysis can also be used to degrade complex organic molecules to yield value added products. Little work has been reported on this issue, like photodegradation of lignin aqueous solution to give valuable products like acetic acid and succinic acid[76].

iv. Majority of the works in photocatalysis are carried out in batch mode. Thus there is an urge for the design of a prototype for the convenience of photocatalytic degradation of pollutants in the continuous mode as well as particle recovery for understanding practical problems associated with it.

2.8 Objectives

The objectives of the present study are

i. To develop a simple cost effective strategy for preparation of photocatalysts to achieve utilization of visible light.

ii. Optimization of catalyst synthesis in order to obtain catalyst with well-defined crystal structure, smaller particle size and high affinity to organic pollutants.

iii. Development of TiO_2 catalyst with high photocatalytic, long term stability and easy regeneration ability.

iv. Characterization of the prepared photocatalyst by advanced analytical techniques like XRD, FESEM, XPS, etc.

v. Study the photocatalytic activity of prepared catalyst via degradation of organic contaminants.

vi. Study the effects of operational parameters on the photocatalytic activity of the prepared photocatalyst.

Chapter 3

3 Experimental Methods

3.1 Experimental Design

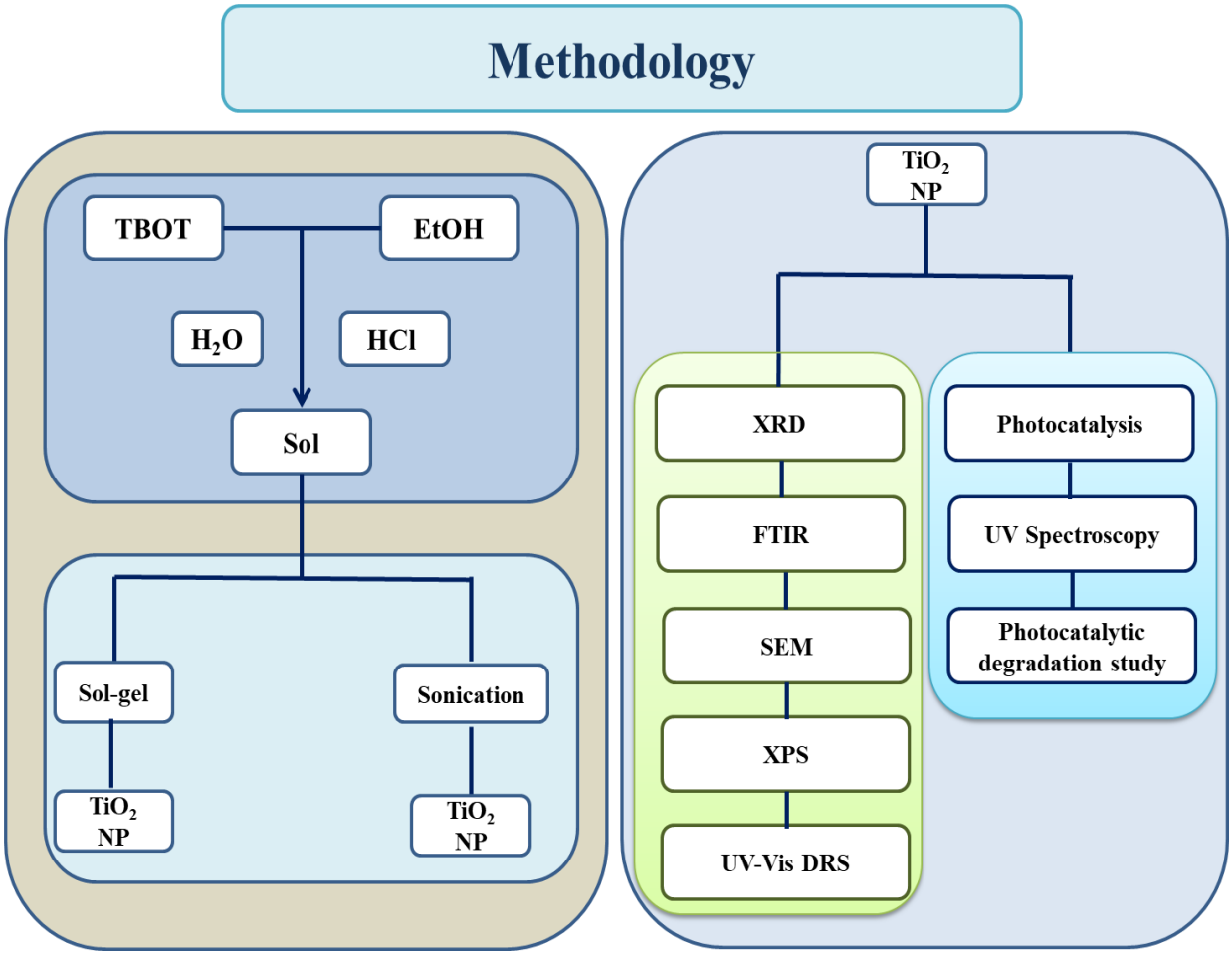

Figure 3 Schematic of overall experimental plan

3.2 Materials and methods

All materials used were of analytical grade. Titanium (IV) butoxide, $Ti(OBu)_4$ 99.7% purchased from Sigma Aldrich was used as titanium source for preparation of titania nanoparticles. Pure ethanol (99%) purchased from Merck was used as solvent. Deionized water was used for the hydrolysis of titanium butoxide and for preparation of all sols and solution. Hydrochloric acid (Merck 95%) was employed as catalyst. Methylene Blue ($C_{16}H_{18}N_3SCl.3H_2O$) obtained from E. Merck, India was used as the model dye without further purification. The solutions were prepared by dissolving the required amount of dye in distilled water.

3.3 Preparation of TiO_2 nanoparticles

Two synthesis methods, sol-gel and ultrasonic method were used for the synthesis of C doped TiO_2 nanoparticles. Titania nanoparticles were obtained via sol-gel route using butoxide as the precursor. In a typical procedure 10ml titanium butoxide was mixed 10ml pure ethanol followed by drop wise addition of 5ml deionized water under constant stirring in room temperature. The pH of the sol was maintained by adding hydrochloric acid. The white sol thus obtained was stirred for 12h and aged for 1 day. The suspension was then centrifuged and washed with deionized water to get the solvent free particles which was kept for drying at 100°C for 12hr. Subsequent calcination of the obtained powder at 250°C resulted in the formation of TiO_2 nanoparticles. For sol gel process, the amount of acid was varied keeping all other synthesis parameters constant. The description of samples of sol gel synthesis is given in the table 3:

Table 3 Sample Description for sol gel synthesis

Name	Amount of acid added (ml)	Calcination Temperature (°C)
T-1	1	250
T-0.75	0.75	250
T-0.5	0.5	250
T-0.25	0.25	250
T-0	0	250

For ultrasonic method, the obtained sol after 15min of initial stirring was sonicated in bath sonicator for different time periods. The aging part as well as the subsequent steps is similar to that of sol gel process. The description of samples of sol gel synthesis is given in the table 4:

Table 4 Sample description for ultrasonic synthesis

Name	Sonication Time(h)	Amount of acid added (ml)
S-0.5	0.5	1
S-1	1	1
S-3	3	1

3.4 Characterizations of prepared photocatalyst

Several techniques were employed for the characterization of the samples. FTIR (Perkin Elmer) was mainly used as a qualitative technique for the study of the surface chemical functional groups on titania nanoparticles. In order to determine the crystal phase composition and the crystallite size of the photocatalysts, X-ray diffraction measurements were carried out at room temperature using a Rigaku Giegerflex D/Max B diffractometer with Cu-K radiation in the region $2\theta=10–80°$. The microcrystalline structure and surface characteristics of the photocatalysts were investigated by using field emission scanning electron microscopy (JEOL JSM-7610F Plus). The powdered samples were placed on a carbon tape and then coated with a thin layer of gold-palladium in an argon atmosphere using agar sputter coater. XPS spectra were taken with PHI Versa Probe III. The shift of the binding energy owing to relative surface charging was corrected using the C1s level at 284.6eV as an internal standard and Ar+ sputtering was employed to clean the surfaces. The UV-is diffuse reflectance spectra (DRS) were measured using a UV-Vis spectrophotometer (Perkin Elmer LAMDA 950) with an integrating sphere attachment and BaSO4 was used as the reference.

3.5 Photocatalytic degradation experiments

The photocatalytic oxidation of methylene blue (MB) in TiO_2 suspension under UV illumination was investigated in order to evaluate the photocatalytic activity of the prepared TiO_2 nanoparticles. Methylene Blue (MB) was chosen as the model dye for the photodegradation experiments. In a typical experiment 0.3g photocatalyst was added under stirring to 100ml of 10mg/L MB dye at pH 10 and kept in dark for 30min to establish the adsorption equilibrium before it was irradiated. The mixture inside a 500 ml beaker remained in suspension by magnetic stirring. A 150W UV lamp was used as UV light source and a water jacket was used to maintain the temperature. A fixed quantity of MB suspension was taken at regular intervals during irradiation period and centrifuged to remove the photocatalyst. The remaining dye in the solution was measured at 664.70 nm with a spectrophotometer (Perkin Elmer Lambda 25). For visible light photocatalysis, a 250W visible range lamp ($\lambda>$ 400nm) was used. Operating parameters such as catalyst loading, dye concentration and time were varied to investigate their effects on the photocatalytic activities of prepared photocatalysts.

Chapter 4

4 Results and Discussion

The TiO_2 photocatalysts prepared using modified sol-gel and sonication routes were further characterized by advanced analytical techniques and results are summarized in this section. It is imperative from the results that a new type of material mainly C-doped titania has been successfully developed in this study through a very simple and cost-effective route which has not been reported by other researchers previously as per author's knowledge. The photocatalytic activity of these newly developed materials showed impressive results under visible light which has been summarized in section 4.2.

4.1 Characterization of prepared photocatalysts via sol gel and sonication routes

4.1.1 XRD analysis

Figure 4 shows XRD patterns of the synthesized photocatalysts by sol gel method. It can be observed that samples T-0.25, T-0.5 and T-0.75 showed distinct anatase peaks. For sample T-1 two peaks corresponding to anatase and rutile phases can be observed. T-0 showed weak anatase peak at 25.49 implying that it is mostly amorphous. As the amount of acid is increased to 0.5ml the anatase peak gets sharper. When the amount of acid is increased to 1ml the rutile phase is observed as the dominant phase. Hence it can be concluded that acid addition helps in the formation of crystal phases.

Figure 5 shows the XRD patterns of photocatalysts prepared via sonication route. While sonication periods of 30min and 1h yielded distinct anatase and rutile peaks, that of 3h showed anatase as the dominating phase. The content of rutile phase (X_R) in the crystalline TiO_2 sample was calculated using the following equation:

$$X_R = \frac{\frac{I_R}{I_A K}}{1+\frac{I_R}{K I_A}}$$

Where I_R is the intensity of the most intense line of the rutile phase for the (110) plane of rutile, I_A is the intensity of the most intense line of anatase phase for (101) plane of anatase and K is a constant equal to 0.79[107]. With increasing sonication time from 0.5h to 3h, the

rutile content was found to increase from 0.459 to 0.54. Hence higher sonication time leads to transformation of anatase to rutile phase of TiO_2.

Table 5 Anatase Rutile content calculation

Sample Name	X_R (Rutile content)	X_A (Anatase content) =1- X_R	Ratio of anatse to rutile content = X_A/X_R
S-0.5	0.459	0.541	1.17
S-1	0.535	0.465	0.869
S-3	0.54	0.46	0.851

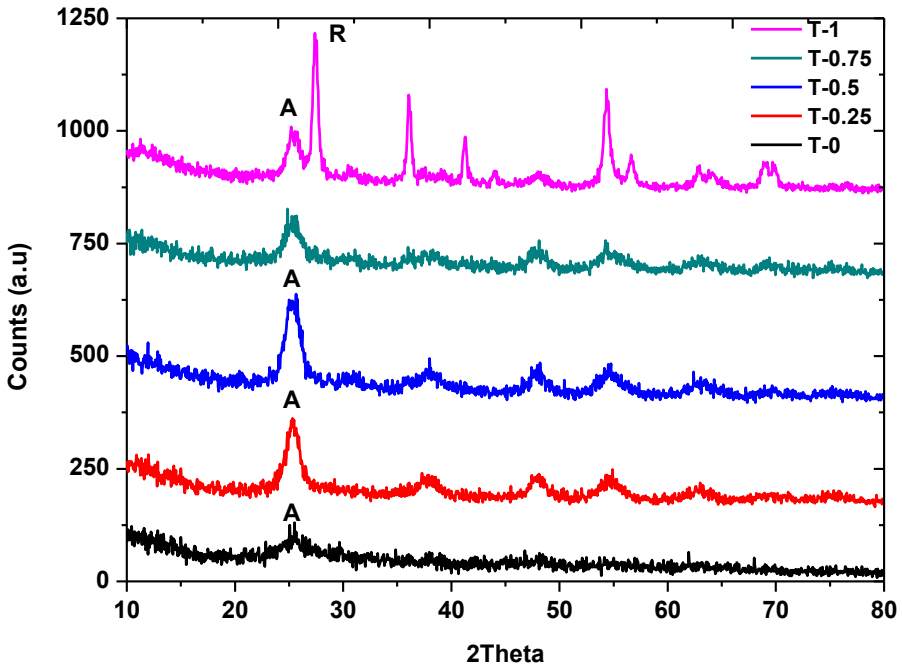

Figure 4 XRD patterns of TiO_2 via sol gel route for varying acid amount

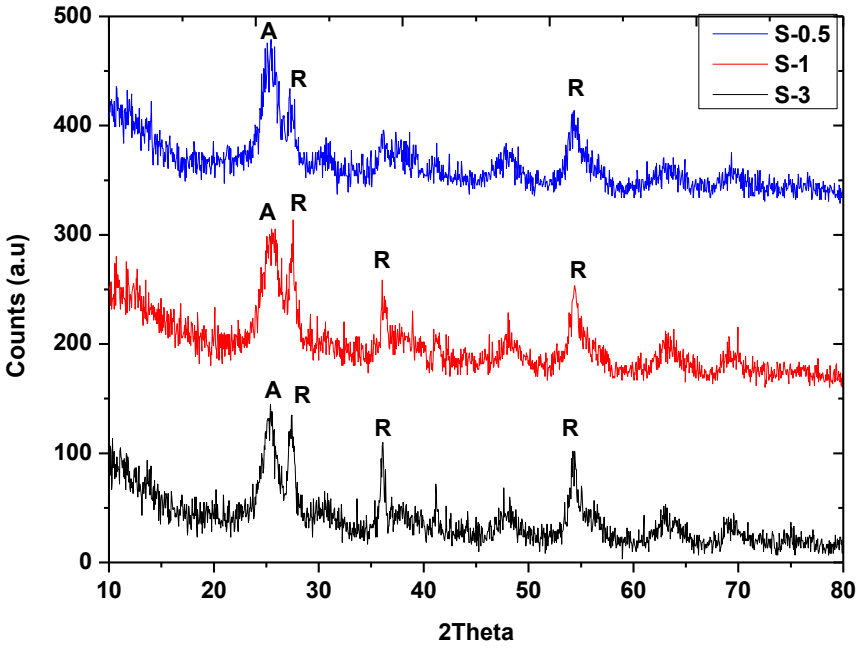

Figure 5 XRD patterns of TiO_2 via sonication route for varying sonication times

4.1.2 FESEM analysis

Figure 6 and Figure 7 shows the morphological features of the titania nanoparticles synthesized by sol-gel and ultrasonic method. As can be seen, for both sol-gel and ultrasonic method the titania particles are spherical in nature. A great degree of agglomeration amongst the nanoparticles was also observed for both the methods.

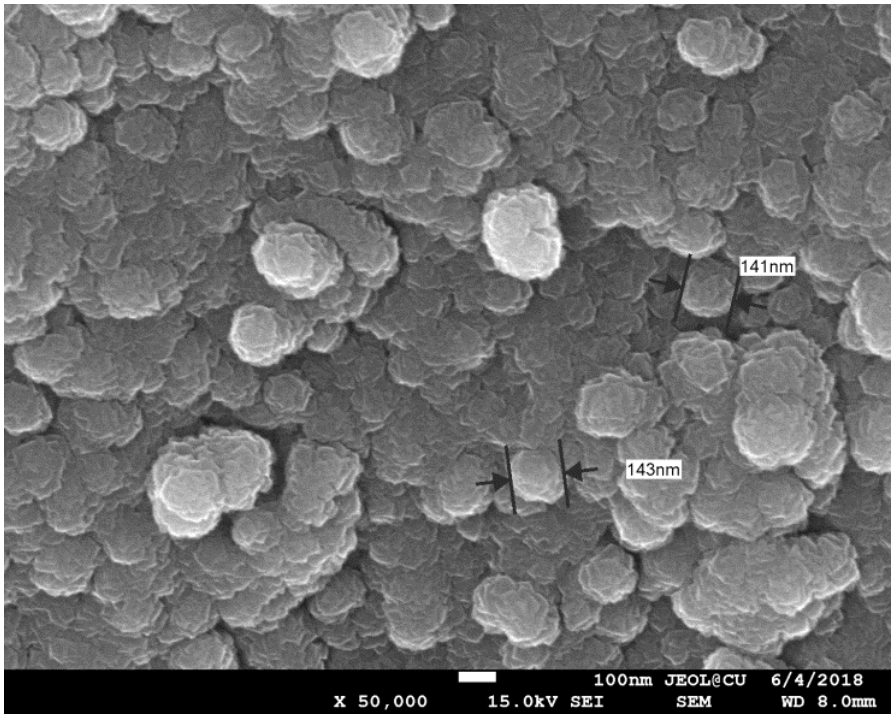

Figure 6 FESEM image of sol gel synthesized TiO_2

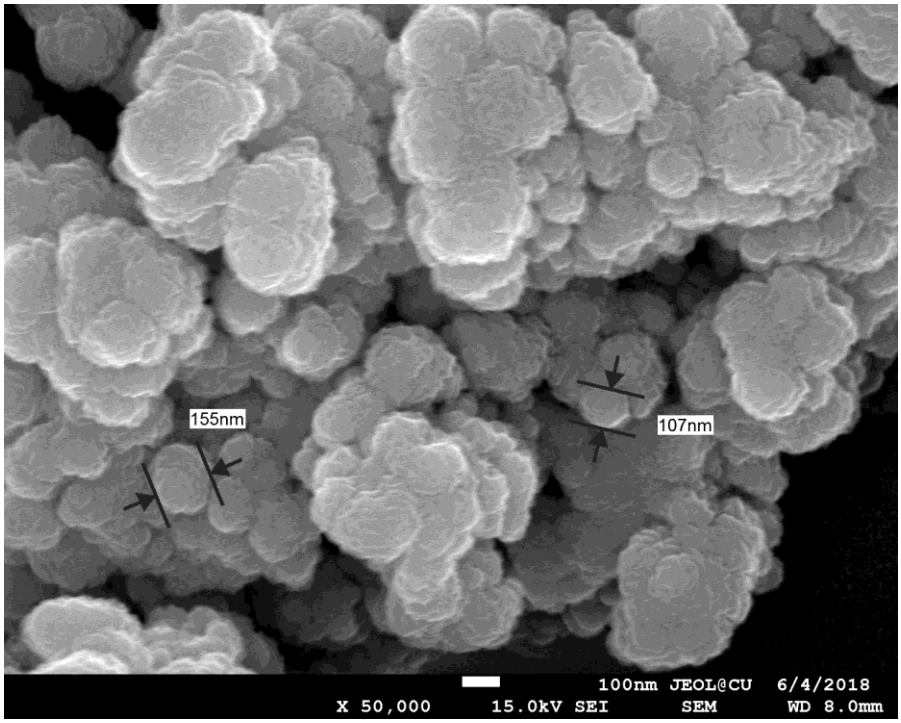

Figure 7 FESEM image of sonication assisted TiO_2

4.1.3 Chemical Analysis

Figure 8 illustrates the survey spectrum for the photocatalyst prepared by both methods. The survey spectra shows distinct characteristic peaks for Titanium, Oxygen and Carbon. From the spectrum it is confirmed that C is present in the samples. This further verifies the results of FTIR spectra. The deconvoluted peaks for different elements are presented in Figures 9-14. The deconvoluted Ti 2p spectrum has 3 peaks centered at around 457eV, 459eV and 463ev. The peaks at 457eV and 463eV are attributed to Ti $2p_{3/2}$ and Ti $2p_{1/2}$[108]. The middle peak around 459eV can be due to presence of Ti^{3+} owing to the Ar^{+} sputtering during XPS measurement[109]. The carbon 1s spectrum reveals 3 peaks at around 283eV, 285eV and 287eV. Peak at 283eV occurs due to elemental carbon and peaks at 285eV and 287eV are similar to those of oxidized carbon species on the surface. Literature suggests that these two peaks refer to the carbonate species as interstitial dopant[110]. The deconvoluted O 1s spectrum has 2 peaks, one at 528eV for Ti-O bond and 530eV for oxygen in hydroxyl or carbonate species.

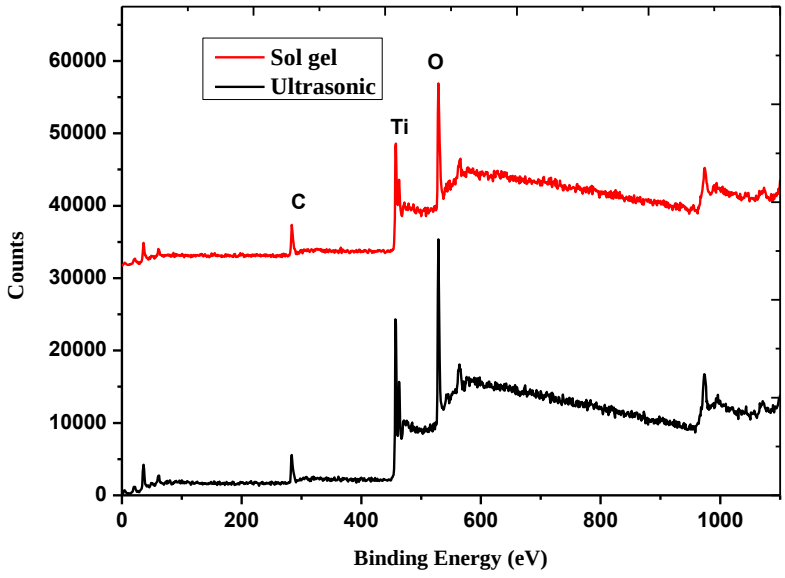

Figure 8 Survey spectra for sol gel and sonicated TiO_2

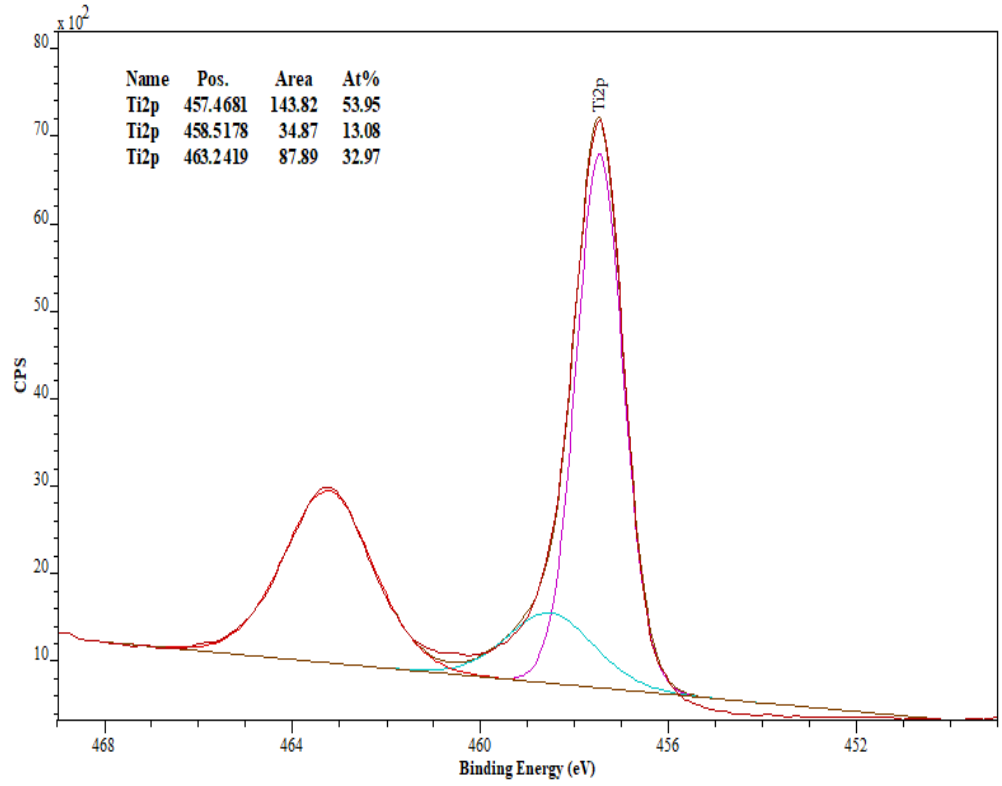

Figure 9 Ti 2p deconvolution for sol gel synthesized TiO_2

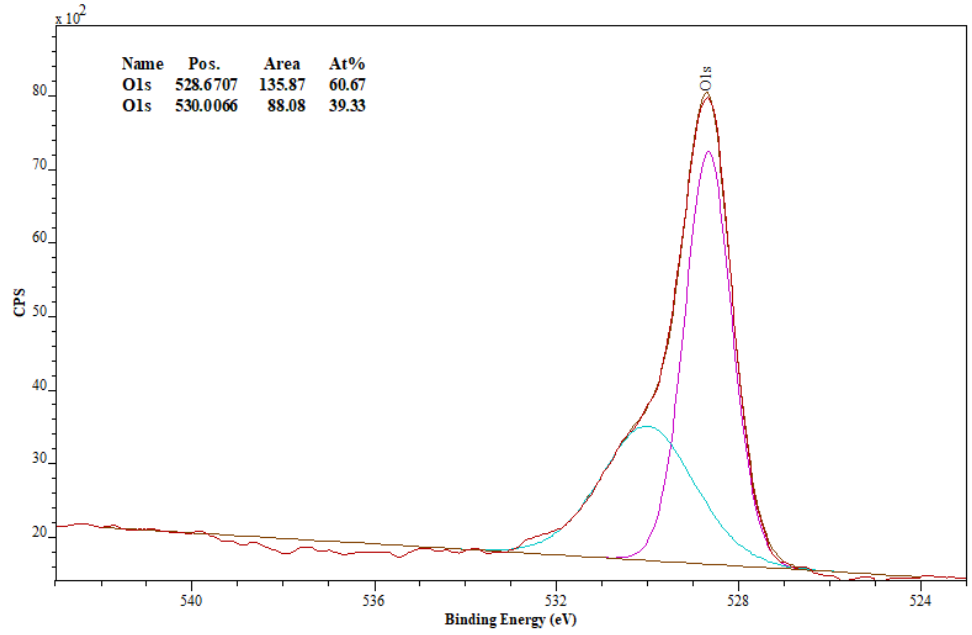

Figure 10 O 1s deconvolution for sol gel synthesized TiO_2

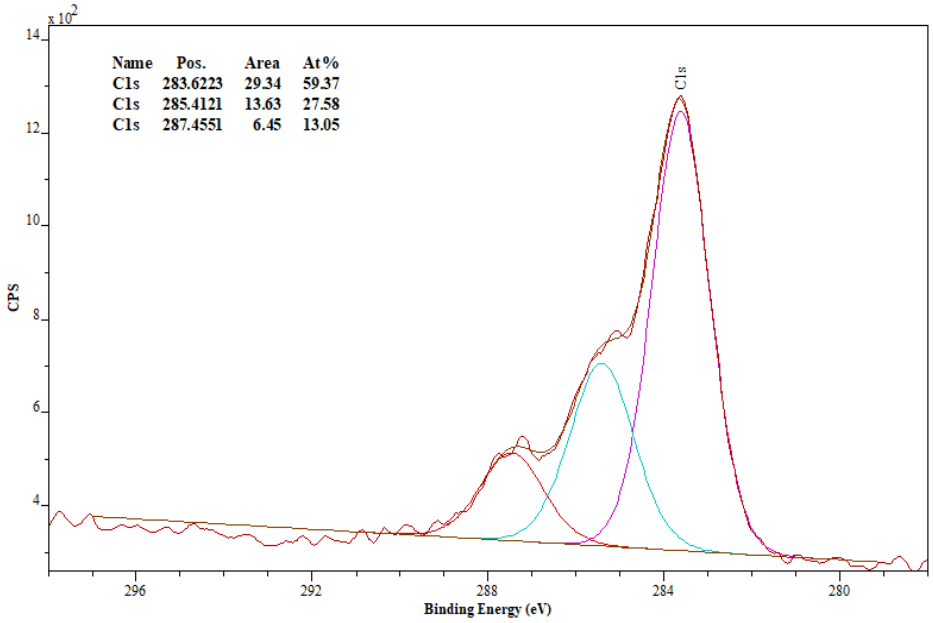

Figure 11 C 1s deconvolution for sol gel synthesized TiO_2

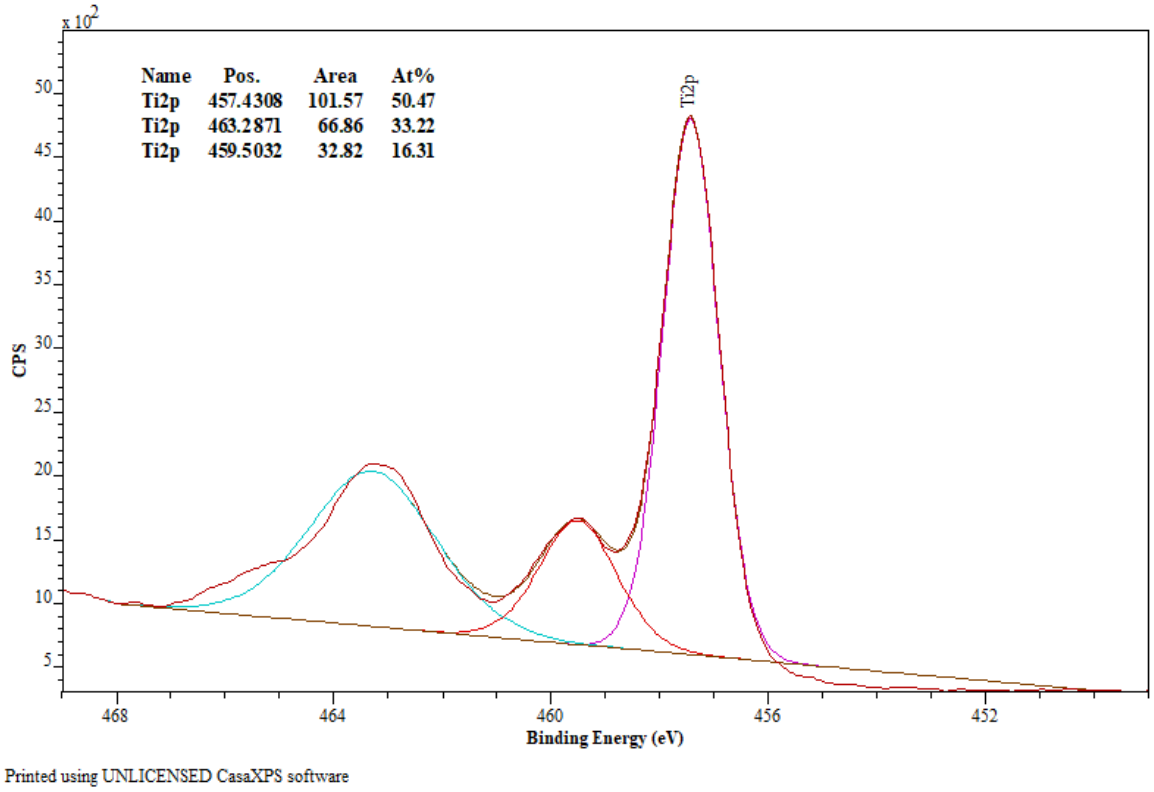

Figure 12 Ti 2p deconvolution for sonicated TiO_2

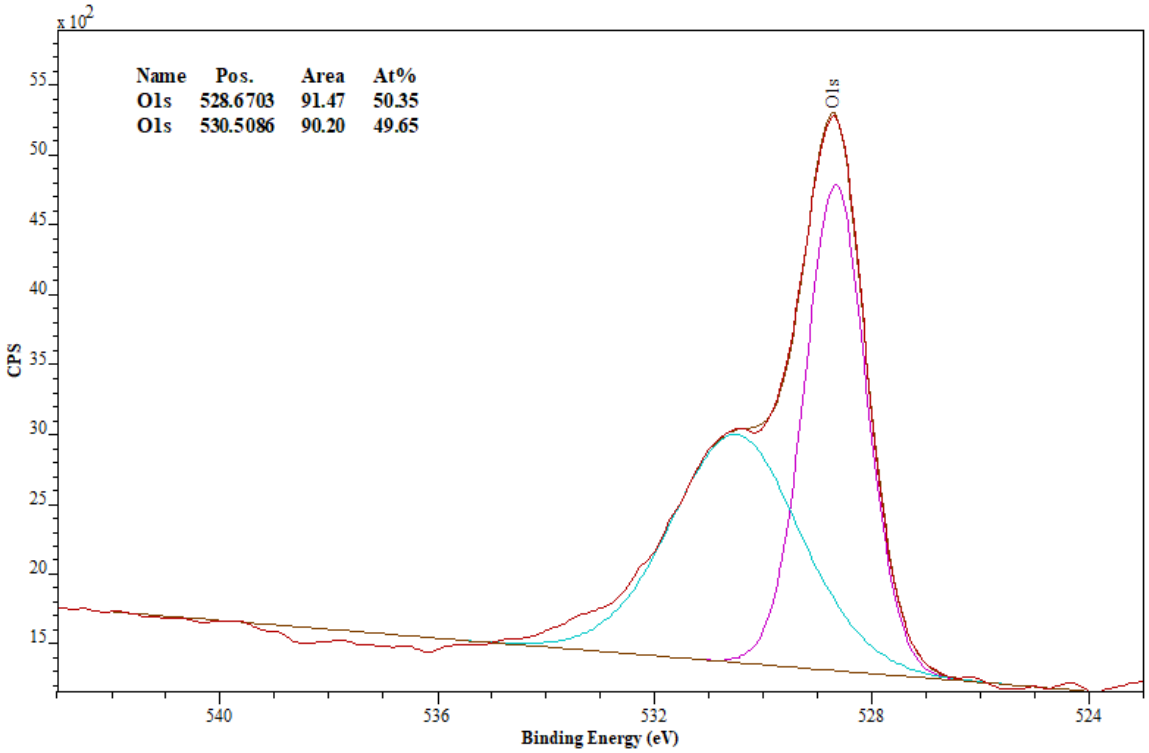

Figure 13 O 1s deconvolution for sonicated TiO_2

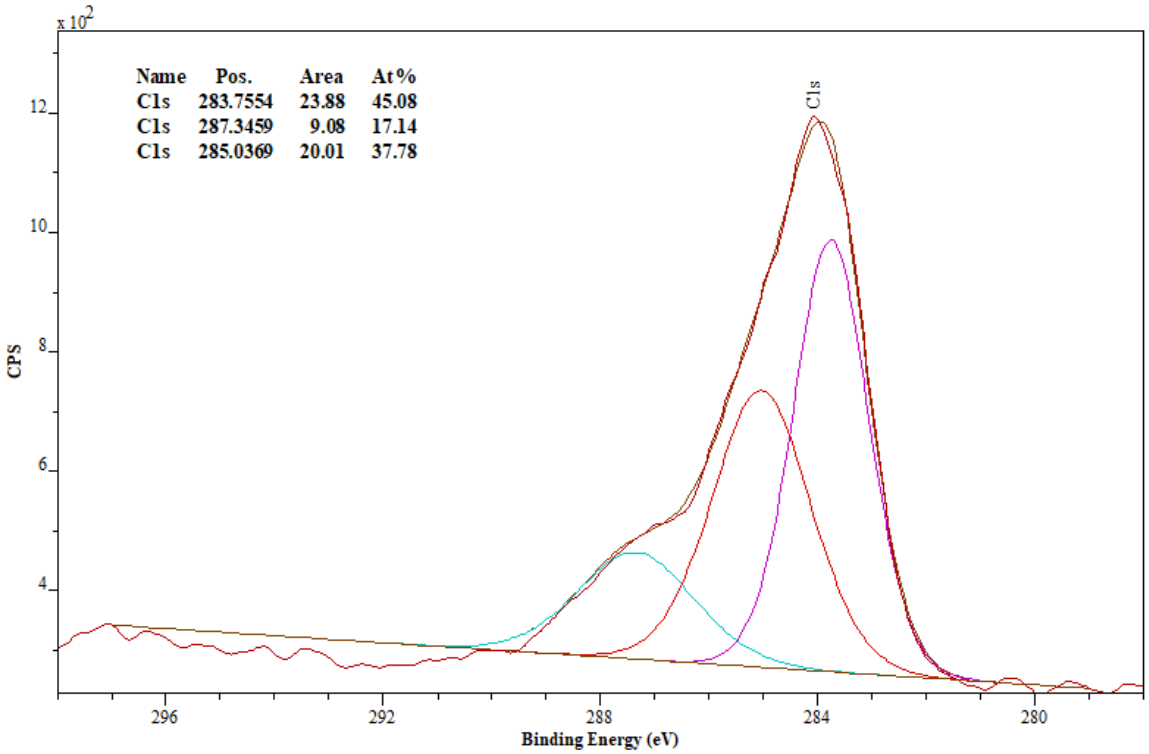

Figure 14 C 1s deconvolution for sonicated TiO_2

4.1.4 FTIR analysis

Figure 15 depicts the FTIR spectrum for the particles in the range of 450cm^{-1} to 4500cm^{-1}. The broad band from 3000cm^{-1} to 3800cm^{-1} corresponds to the vibrations of the hydroxyl O-H groups. The band at 1661cm^{-1} is attributed to bending vibrations of weakly bound water molecules. For both sol-gel and ultrasonic methods there are two bands centered at 2391cm^{-1}, 1510cm^{-1} and 1279cm^{-1}. These corresponds to the stretching vibrations of -CH_3 and -CH_2 groups implying that some organic material is present (most likely from precursor) even after calcination[111]. The broad band centered at 708cm^{-1} is due to the stretching vibrations of Ti-O-Ti[111].

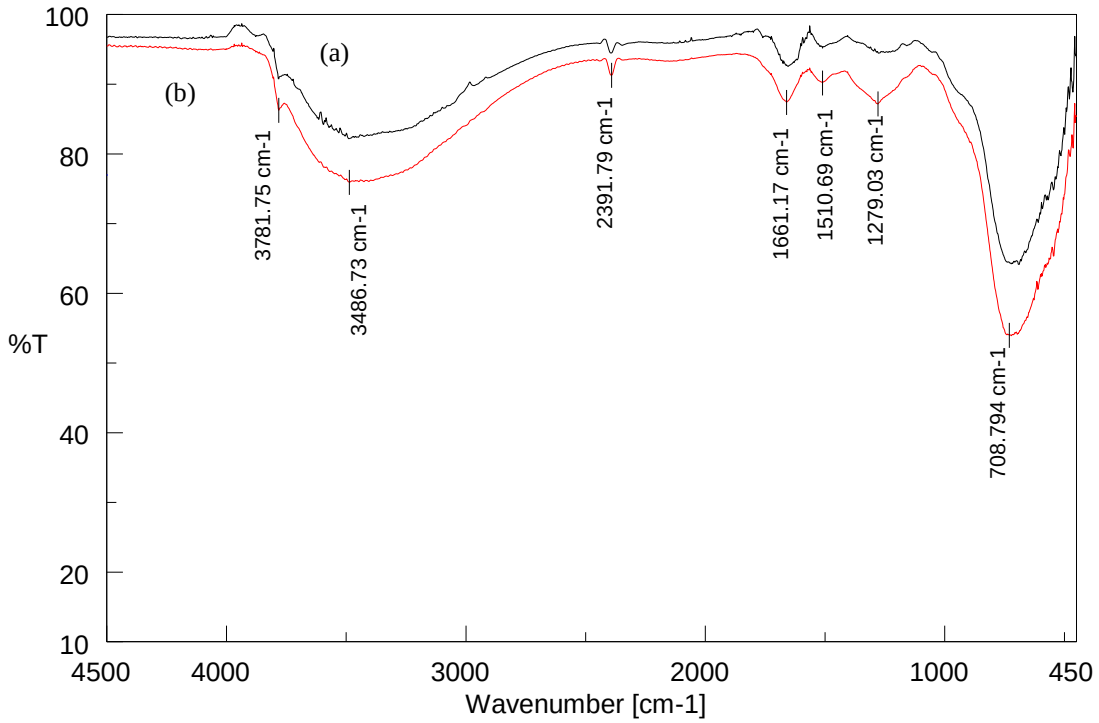

Figure 15 FTIR spectra of TiO_2 nanoparticles synthesized by (a) sol gel and (b) sonication method

4.1.5 UV-Vis Diffuse Reflectance Spectroscopy

In DRS, band gap analysis was performed employing Kubelka–Munk function. The K–M theory is based on a continuum model (Fig. 16), where the reflectance properties for infinitesimally small layers are described by differential equations[112]. Here, the letters I and J represent radiations in the downward and the upward direction, respectively. The downward flux through a layer of thickness dx is decreased by absorption and scattering processes, and increased by scattering process of the light travelling upward towards the surface[113]. Originally, a model known as K-M model was used to describe the behaviour of light travelling inside a light-scattering specimen, which is based on the following differential equations:

$-di = -(S+K)\, i\, dx + S\, j dx$

$dj = -(S+K)\, j\, dx + S\, i dx$

where i and j are the intensities of light travelling inside the sample towards its un-illuminated and illuminated surfaces, respectively; dx is the differential segment along the light path; S and K are respectively called as 'K–M scattering' and 'absorption' coefficients. The last two quantities (S and K) have no direct physical meaning on their own, even though these appear to represent the respective portions of scattered and absorbed lights, per unit vertical length. K–M model holds well when the particle size is comparable to, or smaller than the wavelength of the incident light. In such situation the diffuse reflection no longer allows to separate the contributions of the reflection, refraction, and diffraction, implying that scattering takes place. In the limiting case of an infinitely thick sample, the thickness and sample holder have no influence on the value of reflectance (R). In this case, the K–M equation becomes

$$\frac{K}{S} = \frac{(1-R_\infty)^2}{2R_\infty} = F(R\infty)$$

F(R∞) is the so called remission or Kubelka–Munk function, where $R\infty = R_{sample}/ R_{standard}$. For parabolic band structure, the band gap (Eg), and absorption coefficient (α) of a direct band gap semiconductor, are related through equation as follows $\alpha h\nu = C_1(h\nu - Eg)$ where α is the linear absorption coefficient of the material, hυ is the photon energy and C_1 is a proportionality constant. When the material scatters in perfectly diffuse manner (or when it is illuminated at 601 incidence), the K–M absorption coefficient K becomes equal to 2α

(K=2α). In this situation, considering the K–M scattering coefficient S as constant with respect to wavelength, and using the remission function we can obtain the expression: $[F(R\infty)h\nu]^2 = C_2(h\nu\text{-}Eg)$. Therefore, obtaining F(R∞) and plotting the $[F(R\infty)\ h\upsilon]^2$ against hυ, the band gap Eg of a powder sample can be extracted[113].

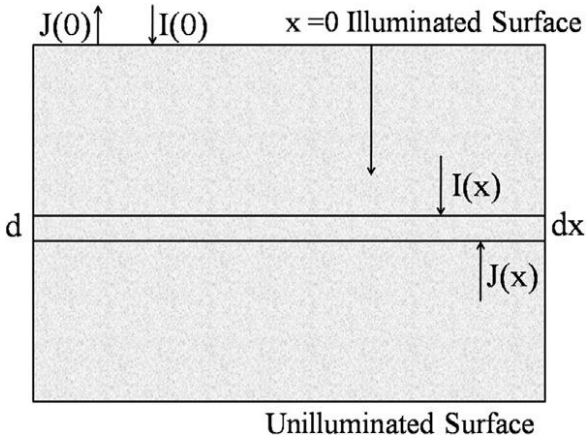

Figure 16 Model for Kubelka Munk analysis

Table 6 shows the obtained band gaps of the prepared photocatalysts. It can be seen that as the amount of acid is increased there is gradual red shift in the band gap of the prepared material. The optimum band gap was found to be 2.8eV; this corresponds to an absorption edge of 442nm. For sonication route higher sonication time periods led to slight increase in band gap. TiO_2 synthesized with 0.5h sonication period has a band gap of 3.0eV having an absorption wavelength of 413nm. Since the absorption edges are greater than 400nm, it can be concluded that the prepared photocatalysts has the ability to absorb visible range light which was further verified by performing photocatalysis experiments as discussed in section 4.2. The diffuse reflectance spectroscopy plots for T-0 and S-0.5 are shown in figure 17 and 18 respectively.

Table 6 Band gap from Kubelka Munk function

Sample Name	Band gap (eV)
T-1	3.07
T-0.75	3.03
T-0.5	2.98
T-0.25	2.90
T-0	2.80
S-3	3.1
S-1	3.06
S-0.5	3.00

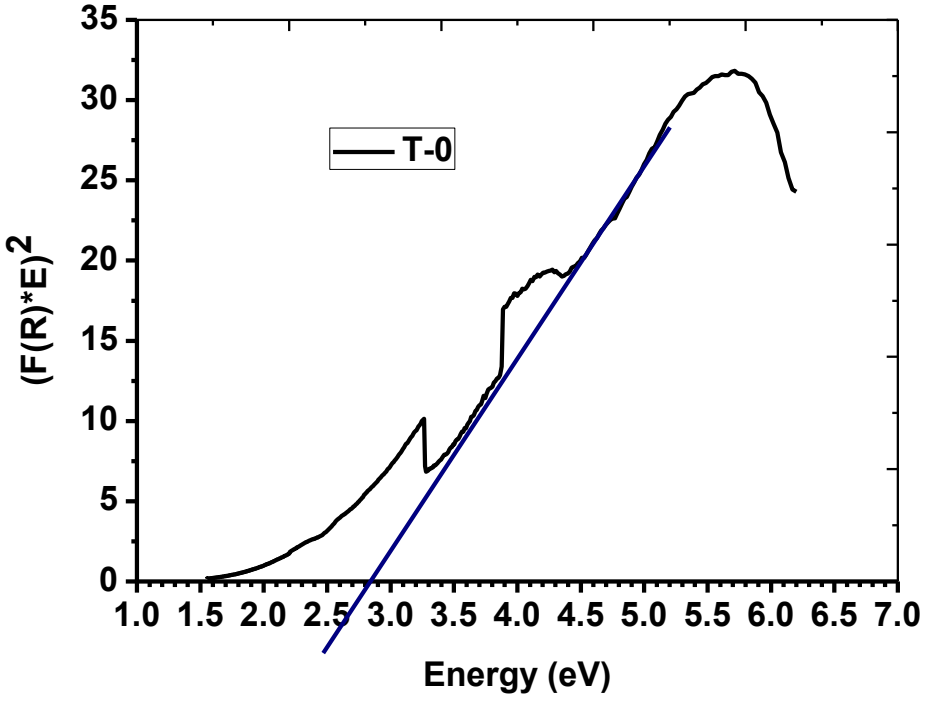

Figure 17 UV-Vis DRS plot for T-0

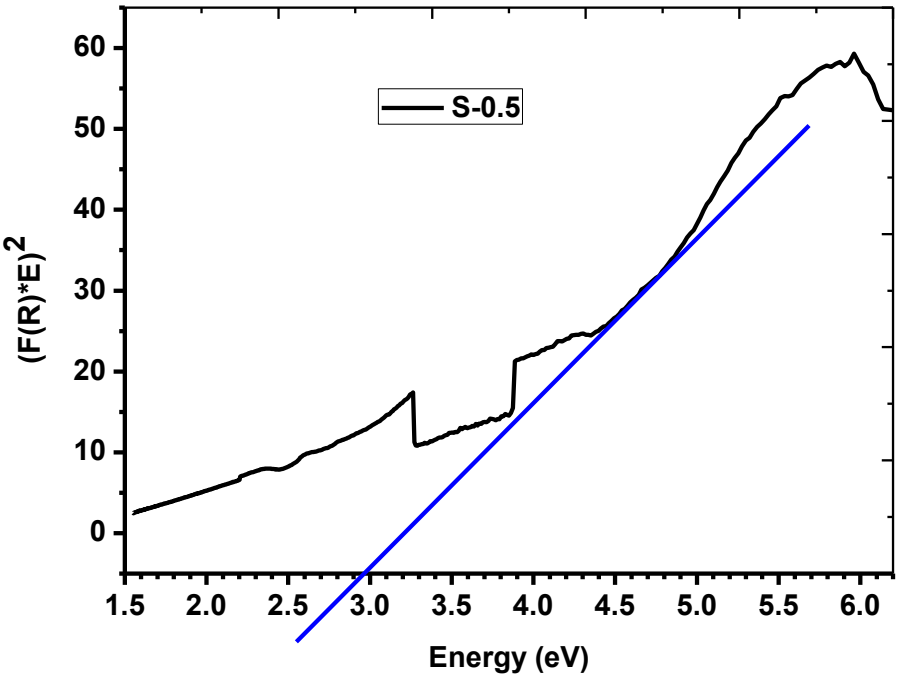

Figure 18 UV-Vis DRS plot for S-0.5

4.2 Photocatalytic performance of prepared photocatalysts

Photocatalytic activity of the prepared materials under UV light, visible light as well as solar light are discussed in this section. The effects of various parameters on photocatalytic performance of the prepared TiO_2 materials are also discussed in details.

4.2.1 Effect of synthesis and operating parameters for synthesized TiO_2

Figure 19 shows the variation in percentage removal of methylene blue dye with varying amount of acid. It can be observed that that the highest removal is obtained with T-0. This agrees well with the UV-Vis DRS results as the sample with lowest band gap is expected to give highest photocatalytic activity. Since T-0 gave highest degradation percentage of 85.8% it was considered optimum and all other experiments were performed with this sample.

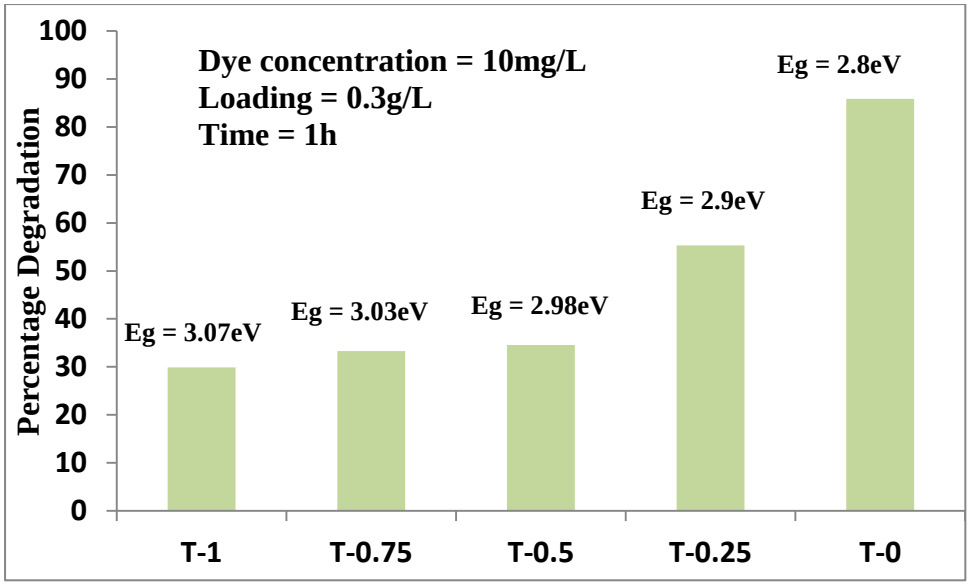

Figure 19 Photocatalytic degradation of methylene blue for varying amounts of acid for solgel method

The variation of photocatalytic activity with sonication time in sonication assisted synthesis of TiO_2 is shown in figure 20. The maximum degradation (22.54%) was observed for sonication time of 0.5h. However there was slight variation in photocatalytic activity with variation in sonication time period. Hence it can be said that sonication method had a greater role in the phase transformation of the crystalline phases and less on the bandgap narrowing of the photocatalyst. The higher degradation percentage for S-0.5 compared to S-1 and S-3 may be attributed with the higher anatase content in S-0.5. Anatase titania is known to exhibit higher photocatalytic activity than rutile phase. Since S-0.5 gave highest degradation percentage of 22.54% it was considered optimum and all other experiments were performed with this sample.

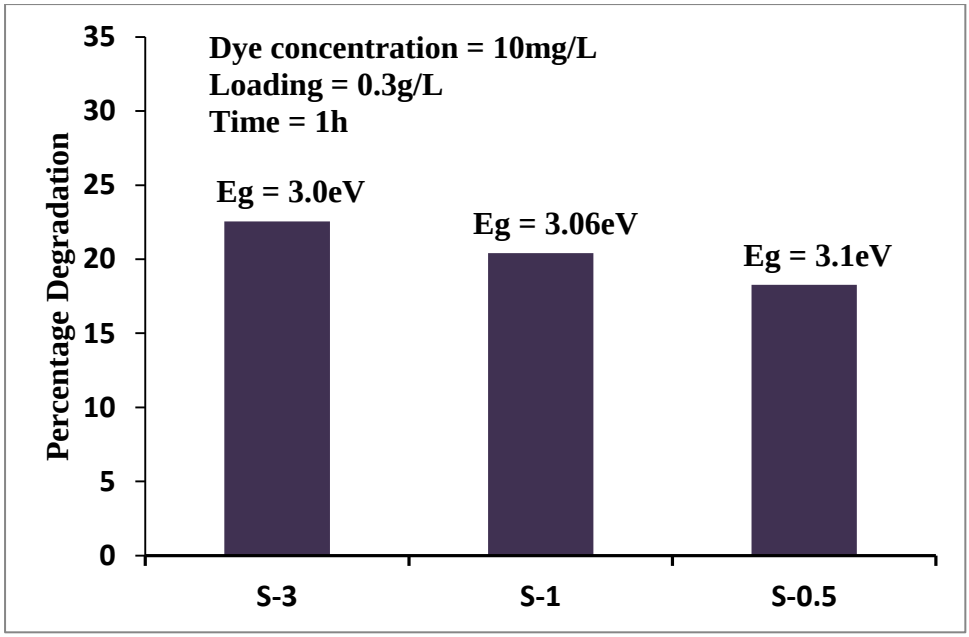

Figure 20 Photocatalytic degradation of methylene blue for varying sonication times for sonication method

Figure 21 displays the effect of loading on the photocatalytic activity. Increase in loading from 0.1g/L to 0.3g/L increases the removal percentage significantly from 60% to 85% for sol gel synthesized TiO_2. The trend for sonication assisted TiO_2 was similar to that of sol gel. This is due the fact that increase in loading not only increases the surface area but also the number of electron hole pairs on light absorption. Similar observations were reported elsewhere[114].

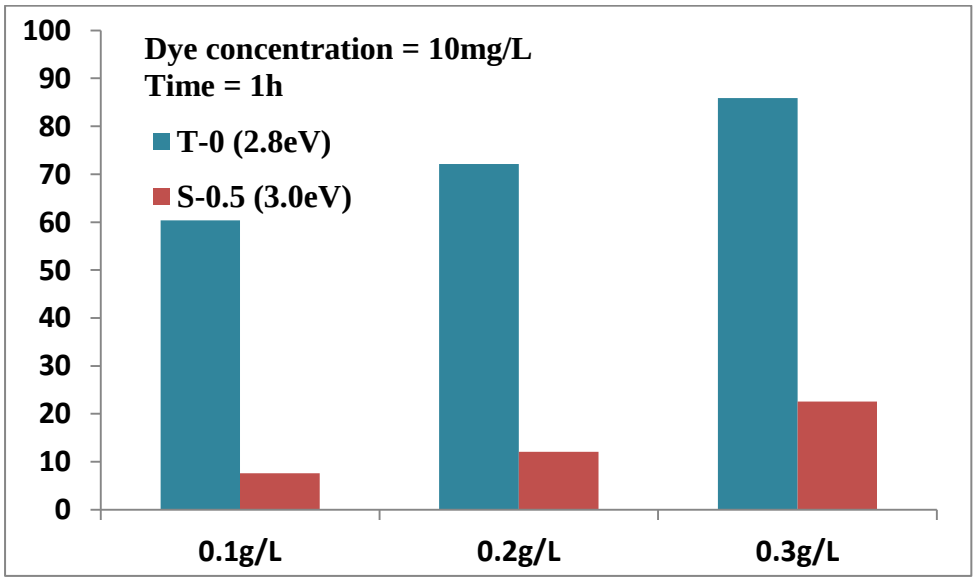

Figure 21 Effect of loading on photocatalytic activity

Figure 22 illustrates the effect of initial dye concentration on photoactivity of TiO_2. The degradation was 95.4% for 5mg/L and then drastically fell to 55% for 30mg/L for sol gel synthesized TiO_2. Here also the trend for sonication assisted TiO2 was similar to that of sol gel. The removal percentage decreased from 34 to 11 when concentration was increased to 30mg/L. The ultraviolet light can penetrate more easily through the solution to irradiate the TiO_2 when the initial dye concentration is lower, therefore, photocatalytic efficiency increased with decreasing initial dye concentration. At high concentrations, large amount of dye are adsorbed on TiO_2 particles which prevented dye molecule reaction with free radical and electron- holes. For this reason, at higher dye concentrations, photonic efficiency is decreased[115]. These results are in good agreement with Ling and Mohamed result[116].

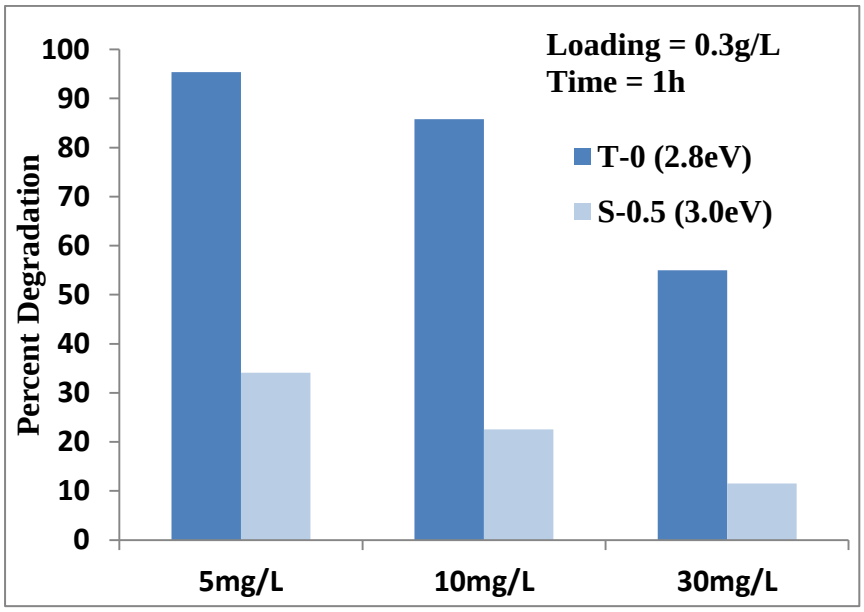

Figure 22 Effect of initial dye concentration

4.2.2 Kinetics of photocatalytic degradation

The heterogeneous reaction includes two consecutive steps. Firstly, the reactants are adsorbed on the surface of the photocatalysts and secondly, the photocatalytic reaction commences. In general, the adsorption rate is slower than the photocatalytic reaction rate. So the overall photocatalytic reaction rate is mainly dominated by the adsorption rate. Furthermore, the adsorption rate can be equivalently expressed using the coverage ratio of the adsorbed reactants on the surface of the photocatalysts[117]. So the photocatalytic reaction rate r can be expressed as the following equation, which is widely known as the original Langmuir-Hinshelwood model.

$$r = -\frac{dc}{dt} = k_p\theta$$

where c is the concentration of the reactant, t is the photocatalytic reaction time, θ is the coverage ratio of pollutants on the TiO_2 surface, k_p is photoreaction coefficient. According to Langmuir adsorption theory, the coverage ratio is related to adsorption capacity and the concentration of the reactant. K_L was defined as adsorption equilibrium constant to measure the adsorption capacity of TiO_2 and coverage ratio θ can be expressed as:

$$\theta = \frac{K_L C}{1+K_L C}$$

Therefore the photoreaction coefficient r can now be expressed as $r = k_p\frac{K_L C}{1+K_L C}$ which can be approximated as $r = -\frac{dC}{dt} = k_{ap}C$. The solution to this first order differential equation with boundary conditions $C=C_0$ at $t= 0$ yields

$$\ln (C_0/C) = k_{ap}t$$

Hence a plot of $\ln (C_0/C)$ versus t yields a straight line with slope $k_{ap.}$

Figure 23 shows the effect of contact time on photocatalytic activity. Before photocatalysis, the solution was kept in dark for 30min to achieve adsorption desorption equilibrium. The dye removal by adsorption was calculated to be 15% within the 30min dark period for T-0 following which complete degradation took place under UV illumination for 1.5h. However for sonication assisted synthesis, the adsorption of dye in the dark period was as low as 5%. Hence it can be said that the surface area of T-0 is greater than that of S-0.5. The kinetics of the photocatalytic reaction was assumed to follow first order and accordingly a plot of $\ln(C_o/C)$ vs t was plotted in figure 24. The plot was linearly fitted with a R^2 value of 0.969 for T-0 and 0.977 for S-0.5 respectively (Figure 24). The corresponding rate constants were found out to be 0.03169 min^{-1} and 0.0029min^{-1}respectively. Hence the rate constant for sol gel method is 10 times that of sonication method. The low rate value can be explained by the high band gap, rutile dominant phase and low surface area of the photocatalyst prepared by sonication method.

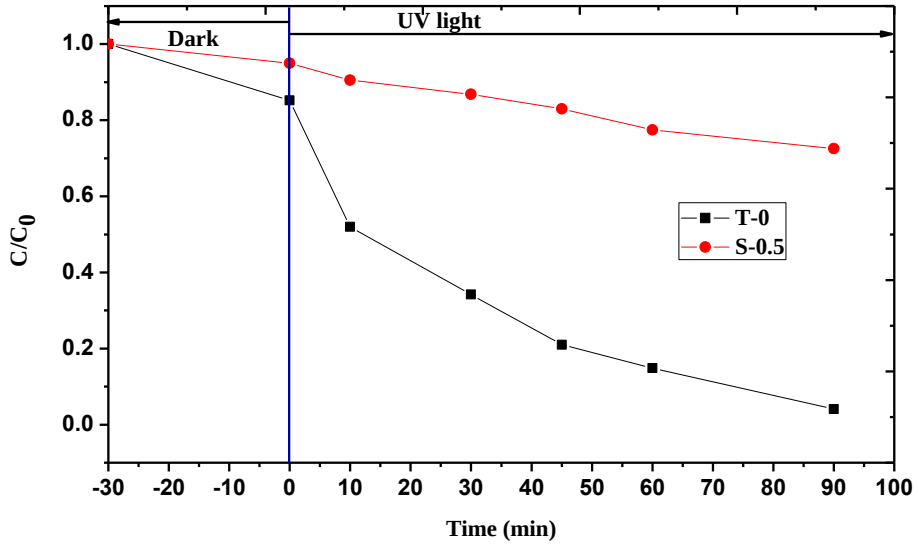

Figure 23 Effect of contact time on photocatalytic degradation

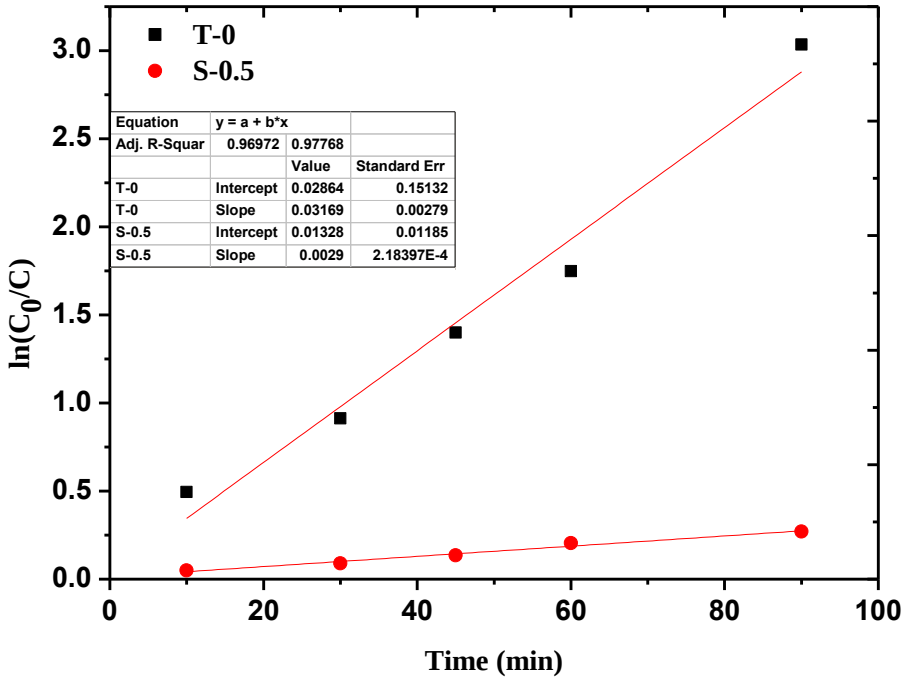

Figure 24 Kinetics of photocatalytic degradation

4.3 Comparison of photocatalyst under ultraviolet, visible and solar radiation

Figure 25 shows the dye degradation under 3 light sources, under ultraviolet, visible and solar radiation. It is seen that both the photocatalysts show photocatalytic activity in visible range. Under solar radiation it took around 30min for 10mg/L of dye solution to be degraded completely. Intensity of solar radiation is much higher than that of 150W UV lamp and 250W visible range lamp, hence the higher degradation percentage.

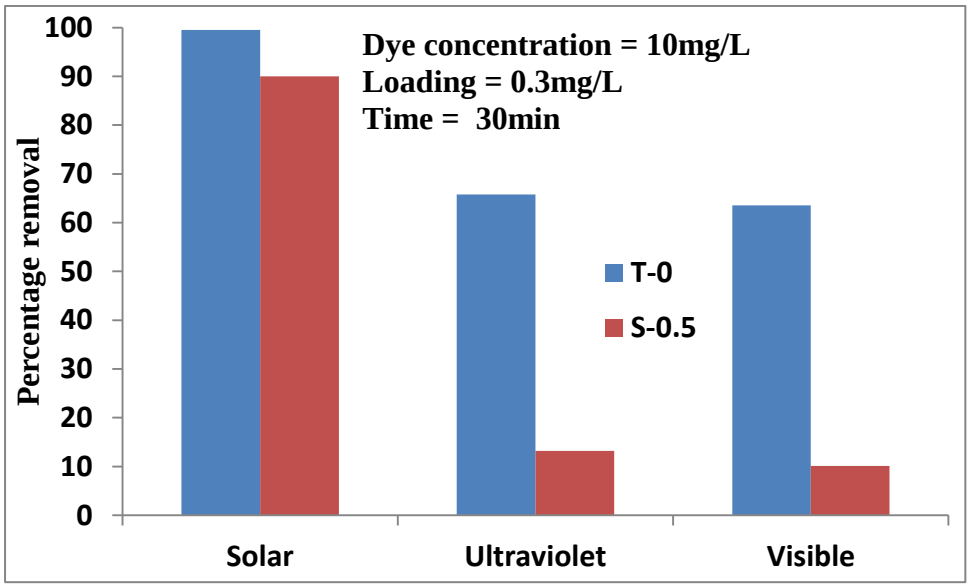

Figure 25 Comparison of photocatalyst under ultraviolet, visible and solar radiation

4.4 Proposed mechanism of formation of photocatalyst

The synthesis, chemistry and structure of metal alkoxides have been a matter of great interest to researchers worldwide. Metal alkoxides react vigorously with water producing metal hydroxides or hydrated oxides. Sol gel process involves complex hydrolysis and condensation reactions which can be summarized as

M-OR + H_2O → M-OH + ROH (Hydrolysis)

M-OH + RO-M → M-O-M + ROH (Condensation)

M-OH + HO-M → M-O-M + H_2O (Condensation)

where M-OR represents the metal alkoxide and R is an alkyl group. During hydrolysis, a hydroxylated alkoxide is produced[118]. The condensation reaction involves removal of

alcohol or water to from M-O-M chains. Hydrolysis of titanium butoxide is vigorous and the polycondensates formed are a function of their physical size and polymeric morphology[119]. During the hydrolytic polycondensation, an inorganic network is formed by a chain of hydrolysis and polycondensation reactions. The oxide network extends as far as the hydrolysis conditions permit. The terminating bonds of this expanding oxide polymer contain OH and OR groups, which make the overall composition of the resultant condensate dependent on the size and polymer morphology[119]. The polycondensed material from titanium or any metal alkoxide can never be 100 per cent oxide since that would require an infinite polymer with no terminal bonds. The rate of conversion of this OH and OR bonds can be modified by varying the water/alkoxide ratio, molecular separation by dilution, hydrolysis medium, catalyst, reaction temperature and other parameters. These OR groups hold the key for carbon doping because without the presence of any external precursor, the only source of carbon is from these terminal OR groups. In general a certain amount of acid is used in sol gel synthesis. The type and amount of acid coupled with other parameters is known to effect the size and crystallinity of the final TiO_2 produced[107]. Two major roles of acid can be obtained from literature. The hydrolytic polycondensation of titanium alkoxides under normal conditions leads to formation and precipitation of particulate materials. Such precipitate formation and self-condensation can be prevented by careful control of molecular interactions during hydrolysis by adding a critical amount of certain acids. The second role of acid is in the formation of crystalline TiO_2. The presence of protons (H^+) may act as a chelating agent, forming a complex with Ti ions and reducing the interaction between the Ti particles. The condensation step is performed more slowly and in a more orderly manner producing crystalline TiO_2[120]. This can be verified from the XRD patterns of sol gel synthesis (Figure 4) that as the amount of acid increases the crystallinity of the sample also increases. It can be inferred that the presence of acid prevents carbon doping into TiO_2 because as the material becomes crystallized, it becomes more difficult for external impurities like carbon to get incorporated in the stable crystal structure. Carbon or any dopant creates additional extrinsic electronic levels in the band gap of TiO_2 resulting in narrowing of the band gap. Sometimes carbon doping is also accompanied by oxygen vacancies which further help in visible light absorption[108]. Normally in sol gel synthesis there is a post calcination step involved. Calcination at high temperature drive off the residual OR groups by combustion and provides the energy for crystallization. In the present work calcination is deliberately done at a low temperature so that there is incomplete combustion of OR groups and some C gets incorporated. From all the discussions above it can be said that higher acid content forbids

lesser C interaction with the crystal structure and hence the band gap is higher. For ultrasonic assisted synthesis, acid content was as high as 1ml and this prevented band gap narrowing. Sonication for higher times created localized hot spots which helped in better hydrolysis and OR content in the oxide network was reduced. Acid content allowed for better crystallization and hence carbon interaction was less, thereby giving higher band gaps than sol gel method. It is also noteworthy to mention that the sample calcined at 250°C had a blackish brown color whereas when the temperature was raised, it turned white. Higher temperature removes the carbon by combustion and so pure white crystalline titania was left behind. The band gap also consequently increased when high temperature was applied. The diffuse reflectance spectrum of T-0 when it was subjected to 500°C is shown in figure 26.

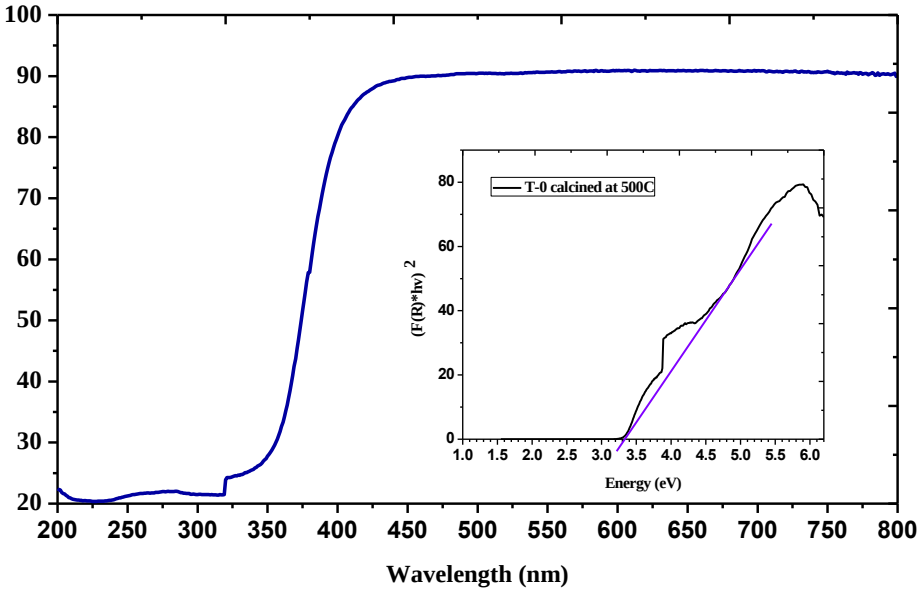

Figure 26 UV-Vis DRS spectra for T-0 when calcined at 500°C

Chapter 5

5 Conclusions

5.1 Conclusions

In the present study, two methods of TiO_2 synthesis, namely sol gel and ultrasonication was adopted for preparation of C doped nanocrystalline titania. The process followed did not involve use of external carbon precursors and was unique, cost effective and simple. Thus it can be considered as a breakthrough in the preparation of C doped TiO_2. The novel material thus prepared displayed significant visible light photocatalysis, thereby overcoming the major drawback of conventional TiO_2. For sol gel method, the amount of acid was varied and for sonication method, sonication time period was varied to investigate their effects on the final photocatalyst. Calcination temperature was lower so that the carbon from OR groups can interact with the band gap of TiO_2 and create additional electronic levels. Carbon doping was thus achieved without using any external precursor. This helped the samples achieve visible light absorption. Photocatalytic activity was evaluated using methylene blue as the model dye. The conclusions from the present study can be summarized as follows:

i. XRD pattern confirmed the crystalline structure both in sol gel synthesized TiO_2 and sonicated TiO_2. Spherical morphology along with agglomeration was observed for the prepared photocatalyst by both the methods. FTIR spectrum revealed the vibrational bonds present in the structure. XPS measurements confirmed the presence of C in the photocatalysts.
ii. For sol gel method higher acid content led to more stable crystalline structure and prevented carbon interaction with TiO_2 thereby reducing the band gap.
iii. For ultrasonic assisted synthesis, higher sonication time failed to lower the band gap. The effect of on sonication was more pronounced on the crystalline structure as it was observed that phase transformation from anatase to rutile took place as sonication time was increased (Table 5).
iv. Higher calcination temperature removed the carbon impurities responsible for visible light absorption and increased the band gap.
v. Lowest band gap (2.8eV) was observed when no acid was used in sol gel method. As for sonication method the band gap varied slightly with sonication time, the average band gap being 3.05eV.

vi. Increase in loading was found to increase the photocatalytic activity since more charge carriers were produced at higher catalyst concentration. As the initial dye concentration was increased, keeping all other parameters constant, the dye removal percentage decreased significantly owing to greater amount of dye molecules in the solution.

vii. Kinetics followed first order model (L-H model) with highest rate constant value of 0.03169 min^{-1} for sol gel method and 0.0029min^{-1} for sonication method. Low surface area and band gap may be the reason behind such low activity of sonicated TiO_2.

viii. The prepared samples showed high degradation values in visible light thus overcoming the greatest drawback of TiO_2 which is its inability to perform in visible light.

5.2 Future prospects

i. In the present study two methods sol gel and ultrasonic method were used to synthesize the nanoparticle. In each of the methods, only one synthesis parameters were varied. However there is considerable scope to obtain better photocatalysts by varying other parameters like alkoxide/water ratio, alkoxide/solvent ratio. The type of solvent and acid can also be varied to study its effect on the final product.

ii. Methylene Blue was used as the model dye to evaluate the photocatalytic activity. However experiments must be carried out with complex organic substances like antibiotics, pesticides. Heavy metal removal for wastewater can also be tried with the prepared photocatalyst.

iii. All the experiments performed in this study are carried out in batch mode. However for industrial applications continuous mode is always preferred, hence continuous reactor has to be designed for practical purposes.

iv. Effect of external dosing like pH, H_2O_2 and ethanol on the photocatalytic removal has to be investigated.

References

[1] J. Schneider *et al.*, “Understanding TiO2 Photocatalysis : Mechanisms and Materials,” *Chem. Rev.*, vol. 114, pp. 9919–9986, 2014.

[2] A. Fujishima, X. Zhang, and D. A. Tryk, “TiO2 photocatalysis and related surface phenomena,” *Surf. Sci. Rep.*, vol. 63, no. 12, pp. 515–582, 2008.

[3] S. Banerjee, S. C. Pillai, P. Falaras, K. E. O’Shea, J. A. Byrne, and D. D. Dionysiou, “New Insights into the Mechanism of Visible Light Photocatalysis,” *J. Phys. Chem. Lett.*, vol. 5, no. 15, pp. 2543–2554, 2014.

[4] V. Etacheri, C. Di Valentin, J. Schneider, D. Bahnemann, and S. C. Pillai, “Visible-light activation of TiO2 photocatalysts: Advances in theory and experiments,” *J. Photochem. Photobiol. C Photochem. Rev.*, vol. 25, pp. 1–29, 2015.

[5] A. Fujishima and K. Honda, “Electrochemical photolysis of water at a semiconductor electrode,” *Nature*, vol. 238, no. 5358, pp. 37–38, 1972.

[6] S. Riyas, V. A. Yasir, and P. N. M. Das, “Crystal structure transformation of TiO2 in presence of Fe2O3 and NiO in air atmosphere,” *Bull. Mater. Sci.*, vol. 25, no. 4, pp. 267–273, 2002.

[7] P. Roy, S. Berger, and P. Schmuki, “TiO2 nanotubes: Synthesis and applications,” *Angewandte Chemie - International Edition*, vol. 50, no. 13. pp. 2904–2939, 2011.

[8] A. M. Valentine, “Titanium: Inorganic & Coordination ChemistryBased in part on the article Titanium: Inorganic & Coordination Chemistry by Charles A. McAuliffe & Neil Bricklebank which appeared in the *Encyclopedia of Inorganic Chemistry, First Edition* .,” *Encycl. Inorg. Chem.*, 2006.

[9] O. Carp, C. L. Huisman, and A. Reller, “Photoinduced reactivity of titanium dioxide,” *Prog. Solid State Chem.*, vol. 32, no. 1–2, pp. 33–177, 2004.

[10] JAMIESON JC and OLINGER B, “Pressure-Temperature Studies of Anatase, Brookite Rutile, and Tio2(Ii). a Discussion,” *Am. Mineral.*, vol. 54, no. 9–10, pp. 1477–1481, 1969.

[11] M. Latroche, L. Brohan, R. Marchand, and M. Tournoux, “New hollandite oxides:

TiO2(H) and K0.06TiO2," *J. Solid State Chem.*, vol. 81, no. 1, pp. 78–82, 1989.

[12] T. L. Thompson and J. T. Yates, "Surface science studies of the photoactivation of TIO2 - New photochemical processes," *Chem. Rev.*, vol. 106, no. 10, pp. 4428–4453, 2006.

[13] X. Chen and S. S. Mao, "Titanium dioxide nanomaterials: Synthesis, properties, modifications and applications," *Chemical Reviews*, vol. 107, no. 7. pp. 2891–2959, 2007.

[14] Q. Zhang, L. Gao, and J. Guo, "Effects of calcination on the photocatalytic properties of nanosized TiO2 powders prepared by TiCl4 hydrolysis," *Appl. Catal. B Environ.*, vol. 26, no. 3, pp. 207–215, 2000.

[15] A. Sclafani, L. Palmisano, and M. Schiavello, "Influence of the Preparation Methods of TiO2 on the Photocatalytic Degradation of Phenol in Aqueous Dispersion," *J. Phys. Chem.*, vol. 94, pp. 829–832, 1990.

[16] A. L. Linsebigler, G. Lu, and J. T. Yates, "Photocatalysis on TiO2 Surfaces: Principles, Mechanisms, and Selected Results," *Chem. Rev.*, vol. 95, no. 3, pp. 735–758, 1995.

[17] S. Di Mo and W. Y. Ching, "Electronic and optical properties of three phases of titanium dioxide: Rutile, anatase, and brookite," *Phys. Rev. B*, vol. 51, no. 19, pp. 13023–13032, 1995.

[18] J. Muscat, V. Swamy, and N. M. Harrison, "First-principles calculations of the phase stability of TiO2," *Phys. Rev. B - Condens. Matter Mater. Phys.*, vol. 65, no. 22, pp. 2241121–22411215, 2002.

[19] K. Tanaka, M. F. V Capule, and T. Hisanaga, "Effect of crystallinity of TiO2on its photocatalytic action," *Chem. Phys. Lett.*, vol. 187, no. 1–2, pp. 73–76, 1991.

[20] A. Selloni, "Crystal growth: Anatase shows its reactive side," *Nature Materials*, vol. 7, no. 8. pp. 613–615, 2008.

[21] W. Wunderlich, T. Oekermann, L. Miao, N. T. Hue, S. Tanemura, and M. Tanemura, "Electronic properties of Nano-porous TiO2- and ZnO-Thin Films-comparison of simulations and experiments," *J. Ceram. Process. Res.*, vol. 5, no. 4, pp. 343–354,

2004.

[22] A. Paxton and L. Thiên-Nga, “Electronic structure of reduced titanium dioxide,” *Phys. Rev. B - Condens. Matter Mater. Phys.*, vol. 57, no. 3, pp. 1579–1584, 1998.

[23] S. Banerjee, J. Gopal, P. Muraleedharan, a K. Tyagi, and B. Raj, “Physics and chemistry of photocatalytic titanium dioxide : Visualization of bactericidal activity using atomic force microscopy,” *Curr. sciense*, vol. 90, no. 10, pp. 1378–1383, 2006.

[24] G. Li, L. Chen, M. E. Graham, and K. A. Gray, “A comparison of mixed phase titania photocatalysts prepared by physical and chemical methods: The importance of the solid-solid interface,” *J. Mol. Catal. A Chem.*, vol. 275, no. 1–2, pp. 30–35, 2007.

[25] B. S. Richards, “Single-material TiO2 double-layer antireflection coatings,” *Sol. Energy Mater. Sol. Cells*, vol. 79, no. 3, pp. 369–390, 2003.

[26] S. Kaur and V. Singh, “Visible light induced sonophotocatalytic degradation of Reactive Red dye 198 using dye sensitized TiO2,” *Ultrason. Sonochem.*, vol. 14, no. 5, pp. 531–537, 2007.

[27] M. Saquib and M. Muneer, “TiO2/mediated photocatalytic degradation of a triphenylmethane dye (gentian violet), in aqueous suspensions,” *Dye. Pigment.*, vol. 56, no. 1, pp. 37–49, 2003.

[28] U. G. Akpan and B. H. Hameed, “Parameters affecting the photocatalytic degradation of dyes using TiO2-based photocatalysts: A review,” *Journal of Hazardous Materials*, vol. 170, no. 2–3. pp. 520–529, 2009.

[29] J. Fan *et al.*, “Dye-sensitized solar cells based on TiO2nanoparticles/nanobelts double-layered film with improved photovoltaic performance,” *Appl. Surf. Sci.*, vol. 319, no. 1, pp. 75–82, 2014.

[30] P. Cheng *et al.*, “TiO2-graphene nanocomposites for photocatalytic hydrogen production from splitting water,” *Int. J. Hydrogen Energy*, vol. 37, no. 3, pp. 2224–2230, 2012.

[31] Y. H. Hu, “A highly efficient photocatalyst-hydrogenated black TiO2 for the photocatalytic splitting of water,” *Angew. Chemie - Int. Ed.*, vol. 51, no. 50, pp. 12410–12412, 2012.

[32] S. U. M. Khan, M. Al-Shahry, and W. B. Ingler, “Efficient photochemical water splitting by a chemically modified n-TiO2,” *Science (80-.).*, vol. 297, no. 5590, pp. 2243–2245, 2002.

[33] M. Kitano, M. Takeuchi, M. Matsuoka, and J. M. Thomas, “Photocatalytic water splitting using Pt-loaded visible light-responsive TiO2 thin film photocatalysts,” *Catal. Today*, vol. 120, no. 2, pp. 133–138, 2007.

[34] J. Bai and B. Zhou, “Titanium dioxide nanomaterials for sensor applications,” *Chemical Reviews*, vol. 114, no. 19. pp. 10131–10176, 2014.

[35] Y. Liu and Y. Yang, “Recent Progress of TiO2 -Based Anodes for Li Ion Batteries,” *J. Nanomater.*, vol. 2016, no. 2, pp. 1–15, 2016.

[36] X. Lu *et al.*, “Hydrogenated TiO2 nanotube arrays for supercapacitors,” *Nano Lett*, vol. 12, no. 3, pp. 1690–1696, 2012.

[37] K. Liu, M. Cao, A. Fujishima, and L. Jiang, “Bio-inspired titanium dioxide materials with special wettability and their applications,” *Chemical Reviews*, vol. 114, no. 19. pp. 10044–10094, 2014.

[38] R. Garcia-Contreras *et al.*, “Effects of TiO2 nanoparticles on cytotoxic action of chemotherapeutic drugs against a human oral squamous cell carcinoma cell line,” *In Vivo (Brooklyn).*, vol. 28, no. 2, pp. 209–215, 2014.

[39] S. M. Gupta and M. Tripathi, “A review of TiO2 nanoparticles,” *Chinese Sci. Bull.*, vol. 56, no. 16, pp. 1639–1657, 2011.

[40] A. Mills and S. Le Hunte, “An overview of semiconductor photocatalysis,” *J. Photochem. Photobiol. A Chem.*, vol. 108, no. 1, pp. 1–35, 1997.

[41] D. W. Bahnemann, C. Kormann, and M. R. Hoffmann, “Preparation and characterization of quantum size zinc oxide: a detailed spectroscopic study,” *J. Phys. Chem.*, vol. 91, no. 14, pp. 3789–3798, 1987.

[42] K. Sivula, F. Le Formal, and M. Grätzel, “WO3-Fe2O3 photoanodes for water splitting: A host scaffold, guest absorber approach,” *Chem. Mater.*, vol. 21, no. 13, pp. 2862–2867, 2009.

[43] X. Chen and A. Selloni, “Introduction: Titanium dioxide (TiO2) nanomaterials,” *Chemical Reviews*, vol. 114, no. 19, pp. 9281–9282, 2014.

[44] R. Verma, J. Gangwar, and A. K. Srivastava, “Multiphase TiO $_2$ nanostructures: a review of efficient synthesis, growth mechanism, probing capabilities, and applications in bio-safety and health,” *RSC Adv.*, vol. 7, no. 70, pp. 44199–44224, 2017.

[45] Y. Wang and Y. Xia, “Bottom-up and top-down approaches to the synthesis of monodispersed spherical colloids of low melting-point metals,” *Nano Lett.*, vol. 4, no. 10, pp. 2047–2050, 2004.

[46] Y. Wang and G. Cao, “Synthesis and enhanced intercalation properties of nanostructured vanadium oxides,” *Chemistry of Materials*, vol. 18, no. 12. pp. 2787–2804, 2006.

[47] C. N. R. Rao, S. R. C. Vivekchand, K. Biswas, and A. Govindaraj, “Synthesis of inorganic nanomaterials,” *Dalt. Trans.*, no. 34, p. 3728, 2007.

[48] Ebelmen, “Untersuchungen über die Verbindungen der Borsäure und Kieselsäure mit Aether,” *Justus Liebigs Ann. Chem.*, vol. 57, no. 3, pp. 319–355, 1846.

[49] G. Oskam, A. Nellore, R. L. Penn, and P. C. Searson, “The Growth Kinetics of TiO 2 Nanoparticles from Titanium(IV) Alkoxide at High Water/ Titanium Ratio,” *J. Phys. Chem. b*, vol. 107, no. Iv, pp. 1734–1738, 2003.

[50] T. Moritz, J. Reiss, K. Diesner, D. Su, and A. Chemseddine, “Nanostructured crystalline TiO2 through growth control and stabilization of intermediate structural building units,” *J. Phys. Chem. B*, vol. 101, no. 41, pp. 8052–8053, 1997.

[51] J. Yu, X. Zhao, and Q. Zhao, “Effect of surface structure on photocatalytic activity of TiO_2 thin films prepared by sol-gel method,” *Thin Solid Films*, vol. 379, no. 1–2, pp. 7–14, 2000.

[52] T. Watanabe, S. Fukayama, M. Miyauchi, A. Fujishima, and K. Hashimoto, “Photocatalytic activity and photo-induced wettability conversion of TiO2 thin film prepared by sol-gel process in a soda-lime glass,” *J. Sol-Gel Sci. Technol.*, vol. 19, no. 1/3, pp. 71–76, 2000.

[53] R. S. Devan, R. A. Patil, J. H. Lin, and Y. R. Ma, “One-dimensional metal-oxide

nanostructures: Recent developments in synthesis, characterization, and applications," *Adv. Funct. Mater.*, vol. 22, no. 16, pp. 3326–3370, 2012.

[54] S. Y. Chae, M. K. Park, S. K. Lee, T. Y. Kim, S. K. Kim, and W. I. Lee, "Preparation of size-controlled TiO2 nanoparticles and derivation of optically transparent photocatalytic films," *Chem. Mater.*, vol. 15, no. 17, pp. 3326–3331, 2003.

[55] Q. Zhang and L. Gao, "Preparation of oxide nanocrystals with tunable morphologies by the moderate hydrothermal method: Insights from rutile TiO2," *Langmuir*, vol. 19, no. 3, pp. 967–971, 2003.

[56] G. C. Richard, C. E. John, and M. Frank, "Sonoelectrochemical processes: A review," *Electroanalysis*, vol. 9, no. 7, pp. 509–522, 1997.

[57] D. J. Walton *et al.*, "Sonovoltammetry at platinum electrodes: surface phenomena and mass transport processes," *J. Appl. Electrochem.*, vol. 25, no. 12, 1995.

[58] Y. Zhu, H. Li, Y. Koltypin, Y. R. Hacohen, and A. Gedanken, "Sonochemical synthesis of titania whiskers andnanotubes," *Chem. Commun.*, no. 24, pp. 2616–2617, 2001.

[59] H. Arami, M. Mazloumi, R. Khalifehzadeh, and S. K. Sadrnezhaad, "Sonochemical preparation of TiO2 nanoparticles," *Mater. Lett.*, vol. 61, no. 23–24, pp. 4559–4561, 2007.

[60] J. C. Yu, L. Zhang, and J. Yu, "Direct sonochemical preparation and characterization of highly active mesoporous TiO2 with a bicrystalline framework," *Chem. Mater.*, vol. 14, no. 11, pp. 4647–4653, 2002.

[61] D. Zhang, L. Qi, J. Ma, and H. Cheng, "Formation of crystalline nanosized titania in reverse micelles at room temperature," *J. Mater. Chem.*, vol. 12, no. 12, pp. 3677–3680, 2002.

[62] K. T. Lim, H. S. Hwang, W. Ryoo, and K. P. Johnston, "Synthesis of TiO2 nanoparticles utilizing hydrated reverse micelles in CO2.," *Langmuir*, vol. 20, no. 16, pp. 2466–2471, 2004.

[63] X. Chen and S. S. Mao, "Titanium dioxide nanomaterials: Synthesis, properties, modifications and applications," *Chem. Rev.*, vol. 107, no. 7, pp. 2891–2959, 2007.

[64] A. B. Corradi *et al.*, “Conventional and microwave-hydrothermal synthesis of TiO2 nanopowders,” *J. Am. Ceram. Soc.*, vol. 88, no. 9, pp. 2639–2641, 2005.

[65] A. V. Murugan, V. Samuel, and V. Ravi, “Synthesis of nanocrystalline anatase TiO2 by microwave hydrothermal method,” *Mater. Lett.*, vol. 60, no. 4, pp. 479–480, 2006.

[66] D. Discovery *et al.*, “Synthesis of TiO 2 nanoparticles by Microwave Assisted Sol- Gel Method,” pp. 580–584, 2017.

[67] Z. Zhang *et al.*, “Microwave degradation of methyl orange dye in aqueous solution in the presence of nano-TiO 2-supported activated carbon (supported-TiO 2/AC/MW),” *J. Hazard. Mater.*, vol. 209–210, pp. 271–277, 2012.

[68] X. Wu, Q. Z. Jiang, Z. F. Ma, and W. F. Shangguan, “Synthesis of titania nanotubes by microwave method,” *Chinese J. Inorg. Chem.*, vol. 22, no. 2, pp. 341–345, 2006.

[69] D. Beydoun, R. Amal, G. Low, and S. McEvoy, “Role of Nanoparticles in Photocatalysis,” *J. Nanoparticle Res.*, vol. 1, pp. 439–458, 1999.

[70] M. R. Hoffmann, S. T. Martin, W. Choi, and D. W. Bahnemann, “Environmental Applications of Semiconductor Photocatalysis,” *Chem. Rev.*, vol. 95, no. 1, pp. 69–96, 1995.

[71] K. Nakata and A. Fujishima, “TiO 2 photocatalysis: Design and applications,” *J. Photochem. Photobiol. C Photochem. Rev.*, vol. 13, no. 3, pp. 169–189, 2012.

[72] A. Fujishima, T. N. Rao, and D. A. Tryk, “Titanium dioxide photocatalysis,” *J. Photochem. Photobiol. C Photochem. Rev.*, vol. 1, no. 1, pp. 1–21, 2000.

[73] M. D. Hernández-Alonso, F. Fresno, S. Suárez, and J. M. Coronado, “Development of alternative photocatalysts to TiO2: Challenges and opportunities,” *Energy Environ. Sci.*, vol. 2, no. 12, p. 1231, 2009.

[74] Y. C. Nah, I. Paramasivam, and P. Schmuki, “Doped TiO2 and TiO2 nanotubes: synthesis and applications,” *Chemphyschem*, vol. 11, no. 13, pp. 2698–2713, 2010.

[75] A. G. Kontos *et al.*, “Photo-induced effects on self-organized TiO2 nanotube arrays: The influence of surface morphology,” *Nanotechnology*, vol. 20, no. 4, 2009.

[76] S.-H. Li, S. Liu, J. C. Colmenares, and Y.-J. Xu, “A sustainable approach for lignin

valorization by heterogeneous photocatalysis," *Green Chem.*, vol. 18, no. 3, pp. 594–607, 2016.

[77] I. M. Arabatzis, T. Stergiopoulos, M. C. Bernard, D. Labou, S. G. Neophytides, and P. Falaras, "Silver-modified titanium dioxide thin films for efficient photodegradation of methyl orange," *Appl. Catal. B Environ.*, vol. 42, no. 2, pp. 187–201, 2003.

[78] M. Anpo, "Use of visible light. Second-generation titanium oxide photocatalysts prepared by the application of an advanced metal ion-implantation method," *Pure Appl. Chem.*, vol. 72, no. 9, 2000.

[79] L. Palmisano, M. Schiavello, A. Sclafani, C. Martin, I. Martin, and V. Rives, "Surface properties of iron-titania photocatalysts employed for 4-nitrophenol photodegradation in aqueous TiO2dispersion," *Catal. Letters*, vol. 24, no. 3–4, pp. 303–315, 1994.

[80] A. Zaleska, "Doped-TiO2: A Review," *Recent Patents Eng.*, vol. 2, no. 3, pp. 157–164, 2008.

[81] I. Bannat, K. Wessels, T. Oekermann, J. Rathousky, D. Bahnemann, and M. Wark, "Improving the photocatalytic performance of mesoporous titania films by modification with gold nanostructures," *Chem. Mater.*, vol. 21, no. 8, pp. 1645–1653, 2009.

[82] V. Iliev, D. Tomova, L. Bilyarska, A. Eliyas, and L. Petrov, "Photocatalytic properties of TiO2 modified with platinum and silver nanoparticles in the degradation of oxalic acid in aqueous solution," *Appl. Catal. B Environ.*, vol. 63, no. 3–4, pp. 266–271, 2006.

[83] Z. Ambrus *et al.*, "Synthesis, structure and photocatalytic properties of Fe(III)-doped TiO2prepared from TiCl3," *Appl. Catal. B Environ.*, vol. 81, no. 1–2, pp. 27–37, 2008.

[84] D. Chen, Z. Jiang, J. Geng, Q. Wang, and D. Yang, "Carbon and nitrogen co-doped TiO2 with enhanced visible-light photocatalytic activity," *Ind. Eng. Chem. Res.*, vol. 46, no. 9, pp. 2741–2746, 2007.

[85] S. M. El-Sheikh *et al.*, "High performance sulfur, nitrogen and carbon doped mesoporous anatase-brookite TiO2 photocatalyst for the removal of microcystin-LR under visible light irradiation," *J. Hazard. Mater.*, vol. 280, pp. 723–733, 2014.

[86] R. Asahi, T. Morikawa, T. Ohwaki, K. Aoki, and Y. Taga, “Visible-light photocatalysis in nitrogen-doped titanium oxides,” *Science (80-.).*, vol. 293, no. 5528, pp. 269–271, 2001.

[87] H. Irie, Y. Watanabe, and K. Hashimoto, “Nitrogen-Concentration Dependence on Photocatalytic Activity of TiO2-xNx Powders,” *J. Phys. Chem. B*, vol. 107, no. 23, pp. 5483–5486, 2003.

[88] T. Ihara, M. Miyoshi, Y. Iriyama, O. Matsumoto, and S. Sugihara, “Visible-light-active titanium oxide photocatalyst realized by an oxygen-deficient structure and by nitrogen doping,” *Appl. Catal. B Environ.*, vol. 42, no. 4, pp. 403–409, 2003.

[89] Z. Zhao and Q. Liu, “Mechanism of higher photocatalytic activity of anatase TiO2 doped with nitrogen under visible-light irradiation from density functional theory calculation,” *J. Phys. D. Appl. Phys.*, vol. 41, no. 2, 2008.

[90] X. Wu *et al.*, “Synthesis of high visible light active carbon doped TiO2 photocatalyst by a facile calcination assisted solvothermal method,” *Appl. Catal. B Environ.*, vol. 142–143, no. October, pp. 450–457, 2013.

[91] S. Sakthivel and H. Kisch, “Daylight Photocatalysis by Carbon-Modified Titanium Dioxide,” *Angew. Chemie - Int. Ed.*, vol. 42, no. 40, pp. 4908–4911, 2003.

[92] M. Pelaez *et al.*, “A review on the visible light active titanium dioxide photocatalysts for environmental applications,” *Appl. Catal. B Environ.*, vol. 125, pp. 331–349, 2012.

[93] M. K. Seery, R. George, P. Floris, and S. C. Pillai, “Silver doped titanium dioxide nanomaterials for enhanced visible light photocatalysis,” *J. Photochem. Photobiol. A Chem.*, vol. 189, no. 2–3, pp. 258–263, 2007.

[94] C. Gunawan, W. Y. Teoh, C. P. Marquis, J. Lifia, and R. Amal, “Reversible Antimicrobial Photoswitching in Nanosilver,” *Small*, vol. 5, no. 3, pp. 341–344, 2009.

[95] P. V Kamat, “Quantum Dot Solar Cells. Semiconductor Nanocrystals as Light Harvesters,” *J. Phys. Chem. C*, vol. 112, no. 48, pp. 18737–18753, 2008.

[96] K. S. Leschkies *et al.*, “Photosensitization of ZnO nanowires with CdSe quantum dots for photovoltaic devices,” *Nano Lett.*, vol. 7, no. 6, pp. 2–7, 2007.

[97] K. Palanivelu, J.-S. Im, and Y.-S. Lee, " Carbon Doping of TiO 2 for Visible Light Photo Catalysis - A review ," *Carbon Lett.*, 2012.

[98] S. U. M. Khan, M. Al-Shahry, and W. B. Ingler, "Efficient photochemical water splitting by a chemically modified n-TiO2," *Science (80-.).*, 2002.

[99] S. Sakthivel and H. Kisch, "Daylight Photocatalysis by Carbon-Modified Titanium Dioxide," *Angew. Chemie - Int. Ed.*, 2003.

[100] Y. Choi, T. Umebayashi, S. Yamamoto, and S. Tanaka, "Fabrication of TiO2 photocatalysts by oxidative annealing of TiC," *J. Mater. Sci. Lett.*, 2003.

[101] I. N. Martyanov, S. Uma, S. Rodrigues, and K. J. Klabunde, "Structural defects cause TiO2-based photocatalysts to be active in visible light," *Chem. Commun.*, 2004.

[102] K. Shankar, M. Paulose, G. K. Mor, O. K. Varghese, and C. A. Grimes, "A study on the spectral photoresponse and photoelectrochemical properties of flame-annealed titania nanotube-arrays," *J. Phys. D. Appl. Phys.*, 2005.

[103] H. Irie, S. Washizuka, and K. Hashimoto, "Hydrophilicity on carbon-doped TiO2 thin films under visible light," *Thin Solid Films*, 2006.

[104] C. Xu, R. Killmeyer, M. L. Gray, and S. U. M. Khan, "Enhanced carbon doping of n-TiO2 thin films for photoelectrochemical water splitting," *Electrochem. commun.*, 2006.

[105] P. R. F. Barnes *et al.*, "TiO2 Photoelectrodes for Water Splitting: Carbon Doping by Flame Pyrolysis?," *Dev. Chem. Eng. Miner. Process.*, vol. 14, no. 1–2, pp. 51–70, 2010.

[106] W. Ren, Z. Ai, F. Jia, L. Zhang, X. Fan, and Z. Zou, "Low temperature preparation and visible light photocatalytic activity of mesoporous carbon-doped crystalline TiO2," *Appl. Catal. B Environ.*, 2007.

[107] A. H. Al-Muhtaseb and M. Khraisheh, "Photocatalytic removal of phenol from refinery wastewater: Catalytic activity of Cu-doped titanium dioxide," *J. Water Process Eng.*, 2015.

[108] Y. T. Lin, C. H. Weng, Y. H. Lin, C. C. Shiesh, and F. Y. Chen, "Effect of C content

and calcination temperature on the photocatalytic activity of C-doped TiO2 catalyst," *Sep. Purif. Technol.*, 2013.

[109] X. Wu *et al.*, "Synthesis of high visible light active carbon doped TiO 2 photocatalyst by a facile calcination assisted solvothermal method," *Appl. Catal. B Environ.*, 2013.

[110] Y. Park, W. Kim, H. Park, T. Tachikawa, T. Majima, and W. Choi, "Carbon-doped TiO2 photocatalyst synthesized without using an external carbon precursor and the visible light activity," *Appl. Catal. B Environ.*, 2009.

[111] Z. Li, Y. Zhu, J. Wang, Q. Guo, and J. Li, "Size-controlled synthesis of dispersed equiaxed amorphous TiO<inf>2</inf> nanoparticles," *Ceram. Int.*, vol. 41, no. 7, pp. 9057–9062, 2015.

[112] A. Sahai, Y. Kumar, V. Agarwal, S. F. Olive-Méndez, and N. Goswami, "Doping concentration driven morphological evolution of Fe doped ZnO nanostructures," *J. Appl. Phys.*, 2014.

[113] R. Kumari, A. Sahai, and N. Goswami, "Effect of nitrogen doping on structural and optical properties of ZnO nanoparticles," *Prog. Nat. Sci. Mater. Int.*, 2015.

[114] M. M. Ba-abbad, A. A. H. Kadhum, A. B. Mohamad, and M. S. Takriff, "Synthesis and Catalytic Activity of TiO 2 Nanoparticles for Photochemical Oxidation of Concentrated Chlorophenols under Direct Solar Radiation," vol. 7, pp. 4871–4888, 2012.

[115] K. Dai, L. Lu, and G. Dawson, "Development of UV-LED / TiO 2 Device and Their Application for Photocatalytic Degradation of Methylene Blue," vol. 22, no. April, pp. 1035–1040, 2013.

[116] M. L. Chin, A. R. Mohamed, and S. Bhatia, "Photodegradation of Methylene Blue Dye in Aqueous Stream Using Immobilized TiO₂ Film Catalyst: Synthesis, Characterization and Activity Studies," *J. Teknol.*, 2004.

[117] P. Sun, J. Zhang, W. Liu, Q. Wang, and W. Cao, "Modification to L-H Kinetics Model and Its Application in the Investigation on Photodegradation of Gaseous Benzene by Nitrogen-Doped TiO2," *Catalysts*, vol. 8, no. 8, p. 326, 2018.

[118] C. Leyva-Porras *et al.*, "Low-temperature synthesis and characterization of anatase

TiO<inf>2</inf> nanoparticles by an acid assisted sol-gel method," *J. Alloys Compd.*, 2015.

[119] B. E. Yoldas, "Hydrolysis of titanium alkoxide and effects of hydrolytic polycondensation parameters," *J. Mater. Sci.*, 1986.

[120] J. Zhu *et al.*, "Nanocrystalline anatase TiO2 photocatalysts prepared via a facile low temperature nonhydrolytic sol-gel reaction of TiCl4 and benzyl alcohol," *Appl. Catal. B Environ.*, 2007.